Journal of Medicinal Chemistry Article

J. Med. Chem. **2010,** *53,* 1937–1950 **1937**
DOI: 10.1021/jm901561u

Biological and Biophysical Properties of the Histone Deacetylase Inhibitor Suberoylanilide Hydroxamic Acid Are Affected by the Presence of Short Alkyl Groups on the Phenyl Ring

Frédérik Oger,[†] Aurélien Lecorgne,[‡] Elisa Sala,[§] Vanessa Nardese,[§] Florence Demay,[†] Soizic Chevance,[‡] Danielle C. Desravines,[∥] Nataliia Aleksandrova,[∥] Rémy Le Guével,[†,¶] Simone Lorenzi,[⊥] Andrea R. Beccari,[⊥] Peter Barath,[#] Darren J. Hart,[∥] Arnaud Bondon,[▽] Daniele Carettoni,[§] Gérard Simonneaux,[‡] and Gilles Salbert*[,†]

[†]*Equipe SPARTE, UMR CNRS 6026-Université Rennes 1, Campus Beaulieu, Bâtiment 13, 35042 Rennes, France, Cedex,* [‡]*Equipe ICMV, UMR CNRS 6226-Université Rennes 1, Campus Beaulieu, Bâtiment 10C, 35042 Rennes, France, Cedex,* [§]*Axxam, San Raffaele Biomedical Science Park via Olgettina 58, 20132 Milan, Italy,* [∥]*Unit of Virus Host-Cell Interactions, UJF-EMBL-CNRS, UMI 3265, 6 rue Jules Horowitz, BP181, 38042 Grenoble, France, Cedex 9,* [⊥]*Dompé SpA Via Campo di Pile, I-67100 L'Aquila, Italy,* [#]*Cancer Research Institute, Slovak Academy of Sciences, Vlarska 7, SK-833 91 Bratislava, Slovak Republic, and* [▽]*Equipe RMN-ILP, Université de Rennes 1, UMR6026 CNRS, Campus de Villejean, Bat 05, 35033 Rennes, France, Cedex.* [¶]*Present address: U522 INSERM, Faculté de Médecine, Campus de Villejean, 35033 Rennes, France*

Received June 2, 2009

Inhibition of histone deacetylases (HDACs) leads to growth arrest, differentiation, or apoptosis of tumor cell lines, suggesting HDACs as promising targets for cancer therapy. At present, only one HDAC inhibitor (HDACi) is used in therapy: suberoylanilide hydroxamic acid (SAHA). Here, we describe the synthesis and biological evaluation of a new series of compounds derived from SAHA by substituting short alkyl chains at various positions of the phenyl ring. Such modifications induced variable effects ranging from partial loss of activity to increased potency. Through molecular modeling, we describe a possible interaction between HDAC7 proline 809, a residue that is strictly conserved within class 2 enzymes only, and the amide group of HDACi, while nuclear magnetic resonance experiments indicated that dimethyl *m*-substitution may stabilize the inhibitor in the active site. Our data provide novel information on the structure−activity relationship of HDACi and suggest new ways for developing second generation SAHA-like molecules.

Introduction

Histone deacetylases (HDACs)[a] are enzymes that catalyze lysine deacetylation in various proteinaceous substrates such as histones. HDACs have been divided into four classes on the basis of their protein sequence homology with yeast (*Saccharomyces cerevisiae*) deacetylase enzymes.[1] Briefly, class 1 HDACs (composed of HDAC1, -2, -3, and -8) are closely related to the yeast transcriptional regulator Rpd3 (reduced potassium dependency 3). Class 2 HDACs, including HDAC4, -5, -7, and -9 (class 2a) and HDAC6 and -10 (class 2b), share domain similarity with yeast histone deacetylase I. The class 3 HDACs form the nicotinamide adenine dinucleotide-dependent Sir2 (silent information regulator or sirtuin) family. In humans, seven members of the Sir2 family have been characterized and ordered in four subclasses.[2] Recently, a separate class of HDACs (class 4), comprising only HDAC11 in mammals, was described.[1]

Because aberrant histone acetylation has been linked to malignant diseases,[3] HDAC inhibitors (HDACi) bear great potential as new antitumor drugs. Indeed, they can induce differentiation, growth arrest, and apoptosis of transformed cells in culture. Many of these agents are effective in inhibiting tumor growth in vivo, and some have entered clinical trials as possible antitumor agents.[4] Class 1 and class 2 HDACs are sensitive to similar inhibitors (HDACi) derived from both natural sources and chemical synthesis. HDACi can be classified into six main groups: short chain fatty acids (e.g., butyrate and valproic acid), hydroxamic acids [e.g., trichostatin A (TSA), suberoylanilide acid (SAHA), and oxamflatin], epoxyketones (e.g., trapoxin and HC-toxin), cyclic peptides (e.g., apicidin and depsipeptide), epoxides (e.g., depudecin), and benzamidines (e.g., MS-27-275).[5] Class 3 HDACs, however, are not sensitive to these HDACi, and specific inhibitors such as sirtinol (Sir2 inhibitor naphtol) have been developed for the specific inactivation of these particular HDACs.[6]

HDAC inhibition has recently been clinically validated as a new therapeutic strategy for cancer treatment with the Food and Drug Administration approval of suberoylanilide hydroxamic acid (SAHA) for the treatment of cutaneous T cell lymphoma.[7] Intense research activities are ongoing in pharmaceutical and academic laboratories toward improving the pharmacokinetic and therapeutic indices of current HDACi. The classic pharmacophores for hydroxamic acid inhibitors consist of three distinct structural motifs: the zinc-binding group, a hydrophobic linker, and a cap group.[8] The X-ray structures of a bacterial HDAC homologue, histone deacetylase-like protein (HDLP),[9] bound to SAHA or TSA, and, more recently, human HDAC8,[10] confirmed that the zinc-binding group interacts with a Zn^{2+} ion at the bottom of a

*To whom correspondence should be addressed. Tel: 33(0)2 23 23 66 25. Fax: 33(0)2 23 23 67 94. E-mail: gilles.salbert@univ-rennes1.fr.

[a]Abbreviations: HDAC, histone deacetylase; HDACi, HDAC inhibitors; SAHA, suberoylanilide acid; SACs, SAHA cap derivatives; STD, saturation transfer difference; TSA, trichostatin A; WaterLOGSY, water−ligand observation with gradient spectroscopy.

© 2010 American Chemical Society

Published on Web 02/09/2010

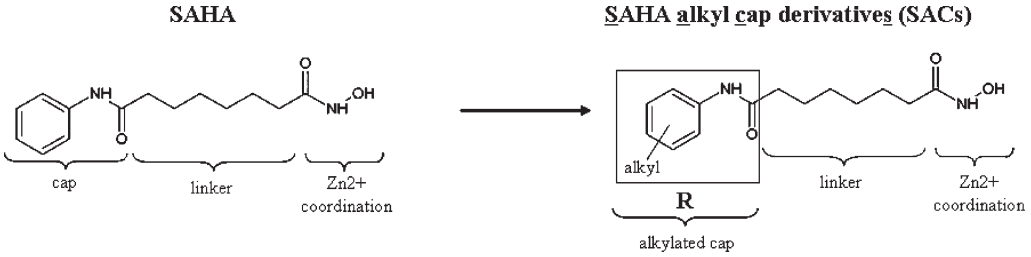

Figure 1. Structure of SAHA and general structure of the synthesized compounds. Compounds were derived from SAHA by substitution with alkyl on the phenyl ring and were named SACs for "SAHA alkyl cap derivatives". SACs conserve the hydroxamic acid function, the length of the aliphatic chain, and the amide function of SAHA and are only modified on the phenyl ring.

channel-like active site. The common zinc-binding group of many HDACi is the hydroxamate moiety, and modifications of this group have been modestly successful, yielding isosteres such as benzamide, α-ketoesters, electrophilic ketones, mercaptoamide, and phosphonates.[8,11] The hydrophobic linker presents the zinc-binding group to the active site, fills the hydrophobic channel, and positions the cap group at the entrance of the active site. The cap group could thus establish interactions with amino acid residues at the rim of the channel.[12] However, in the crystal structure of SAHA in complex with the HDAC7 catalytic domain (PDB ID: 3C0Z), the cap moiety is not well-defined, suggesting that addition of substituents in this part may improve binding and thus efficiency of the HDACi. Hence, targeting of the cap group represents an alternative approach to discovering more potent and/or more selective HDACi such as suggested by Wiest and co-workers using molecular dynamics simulation assays.[13]

Here, we describe the synthesis of a new series of SAHA derivatives harboring alkyl substituents at different positions of the phenyl ring. Our data demonstrate that the biological activity and the biochemical properties of SAHA can be finely modulated by the differential positioning of these substituents.

Results

Chemistry. SAHA cap derivatives (SACs, Figure 1) synthesized and used in this study are depicted in Table 1. All SACs and SAHA were synthesized using the method described by Mai et al.[14] The synthetic route to SAHA analogues is shown in Figure 2. First, suberic anhydride **14** was prepared from a mixture of suberic acid and acetic anhydride in good yield (98%). Then, suberic anhydride was condensed with various aniline derivatives to introduce diversity. In all of the syntheses, we noticed the formation of the expected amide together with the dianilide byproduct (about 10−40%). The latter was removed from solution by precipitation and filtration. The suberanilic acid (**1a**−**13a**) was subsequently treated with hydroxylamine in methanol to give the expected SAHA derivatives (**1**−**13**). Depending on the nature of the aromatic ring, the compounds were obtained in 14−95% yields. All of the compounds were characterized by ^{1}H NMR, ^{13}C NMR, and mass spectrometry. As expected, ^{1}H NMR spectroscopy mainly showed the existence of the *Z*-isomer.[15]

Biological Evaluation. *o*-,*m*-,*p*-Substitutions of the Phenyl Ring Differentially Modulate SAHA's Ability To Inhibit HDACs in Caco-2 Cells. As HDACi are promising drugs to treat colorectal cancer[16,17] (www.clinicaltrials.gov), we analyzed SACs activity in Caco-2 colon cancer cells (Figure 3A,B). Cells were treated with SACs, and the total HDAC activity was then measured. As shown in Figure 3A, the position of substitution impacted the effectiveness of compounds. Indeed, although *p*-substituted compounds

Table 1. List of Synthesized Compounds[a]

		SAHA cap substituent			
		nature	position		
Compound	R		ortho	meta	para
SAHA		/			
1	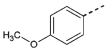	methoxy			✓
2		methyl	✓		
3		methyl		✓	
4		methyl			✓
5		ethyl	✓		
6		ethyl		✓	
7		ethyl			✓
8		dimethyl	✓ **(2)**	✓ **(3)**	
9	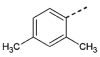	dimethyl	✓		✓
10	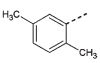	dimethyl	✓ **(2)**	✓ **(5)**	
11		dimethyl	✓ **(2,6)**		
12		dimethyl		✓	✓
13		dimethyl		✓ **(3,5)**	

[a] The position of alkyl substituents on the SAHA phenyl cap is indicated.

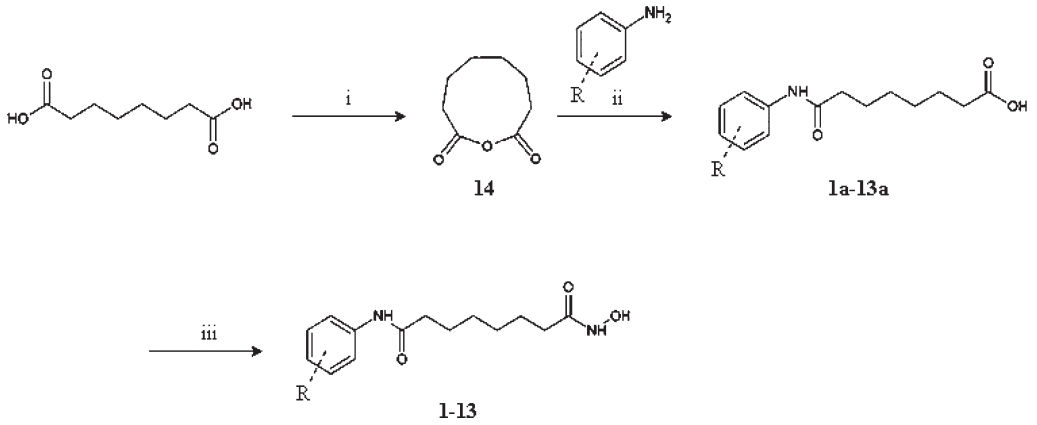

Figure 2. Reagents: (i) Acetic anhydride, 140 °C, 1 h.[31] (ii) THF, room temperature, 30 min. (iii) Ethyl chloroformiate, triethylamine (THF, 0 °C, and 10 min) and then hydroxylamine hydrochloride and potassium hydroxide (MeOH, 0 °C, and 15 min).

(**4** and **7**) were 2-fold less active than SAHA, *m*-substituted compounds (**3** and **6**) were approximately 1.5-fold more active than SAHA. On the contrary, *o*-substituted compounds (**2** and **5**) were 5−10 times less active than SAHA.

We next produced disubstituted compounds. Given that monomethyl and monoethyl substitution of SAHA showed similar effects, only dimethylated SACs were subsequently synthesized. As shown in Figure 3B, the *o*-substituted compound (**11**) was totally inactive toward HDAC inhibition, confirming that *o*-substitution strongly affects SAHA efficiency. HDAC inhibition was partially restored when one *o*-substitution was combined with one *m*- or *p*-substitution (compounds **8**−**10**). Interestingly, the dimethyl-substituted compounds without *o*-substitution (**12** and **13**) were 1.2−3-fold more active than SAHA, respectively. Taken together, these results indicate that alkyl substitution of the SAHA phenyl ring has a profound influence on the effectiveness of the inhibitors.

Position of Alkyl Substituents in SACs Both Quantitatively and Qualitatively Influences Protein Acetylation Levels in Caco-2 Cells. Next, indirect enzyme-linked immunosorbent assays (ELISAs) were performed to monitor the effects of SACs on total protein acetylation levels in Caco-2 cells (Figure 4).The ability of SACs to regulate protein acetylation levels in these cells was in good agreement with their ability to inhibit HDACs (compare Figures 3 and 4). Because different proteins could account for the acetylation signal detected in this assay, the protein acetylation profiles of Caco-2 cells treated with SACs were analyzed by Western blots using antiacetyl lysine antibodies. As shown in Figure 5A, SAHA induced hyperacetylation of proteins previously identified by Sehested and co-workers as α-tubulin and histones.[18] As expected, previously identified active compounds (**1**, **3**, **4**, **6**, and **7**) induced acetylation of these proteins to the same extent as SAHA. Conversely, no *o*-substituted compounds, except **9** and to a lower extent **10**, were able to induce protein hyperacetylation (Figure 5A,B). Compounds **12** and **13** both induced α-tubulin and histone acetylation, although **13** induced only a weak α-tubulin acetylation as compared to SAHA (Figure 5B), suggesting that this particular compound could have a different selectivity than SAHA. These results were directly confirmed by Western blot analysis using antiacetylated α-tubulin and antiacetylated histone H3/H4 antibodies (Supporting Information, S1, S2). Similar results were obtained in the hepatoma cell line HepG2 (Supporting Information, S3).

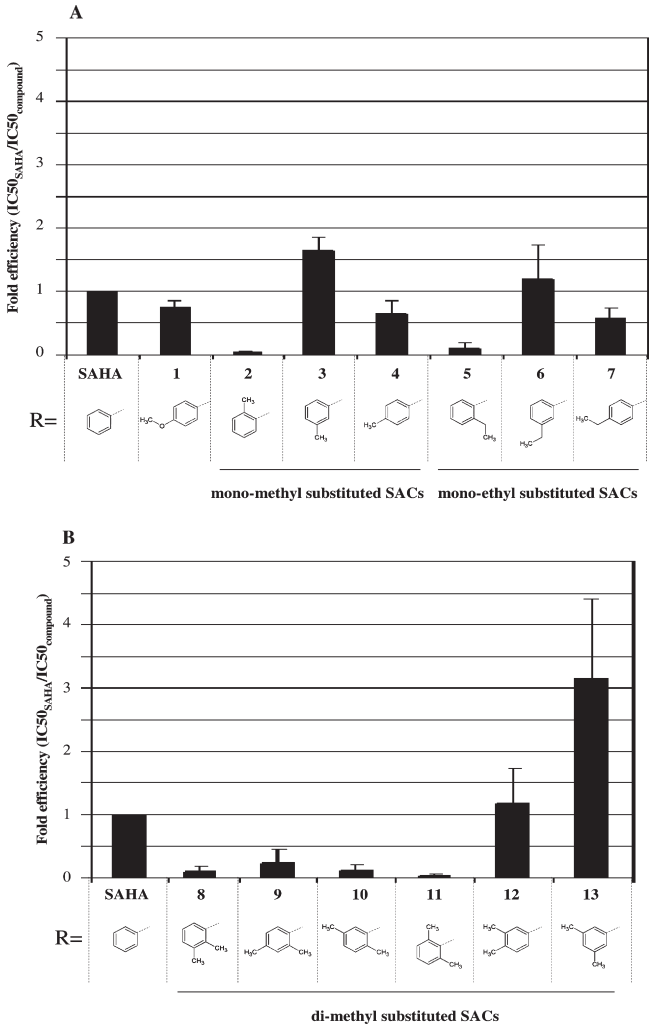

Figure 3. Ex vivo HDAC inhibition in Caco-2 cells in response to treatment with (A) monomethyl- and monoethyl-substituted SACs or (B) dimethyl-substituted SACs. Caco-2 cells were treated in triplicate using increasing concentrations from 0.1 to 50 μM (six concentrations) of the indicated compounds during 4 h. Data are shown as a ratio of IC_{50} values ($IC_{50SAHA}/IC_{50compound}$). Results are the mean of at least three independent experiments except for compound **2** (two independent experiments). Error bars are standard errors of the mean (SEM) except for compound **2** (standard deviation, SD).

Profiling of SACs Efficiency on HDAC1, HDAC3, HDAC5, HDAC6, and HDAC7. To determine the potential

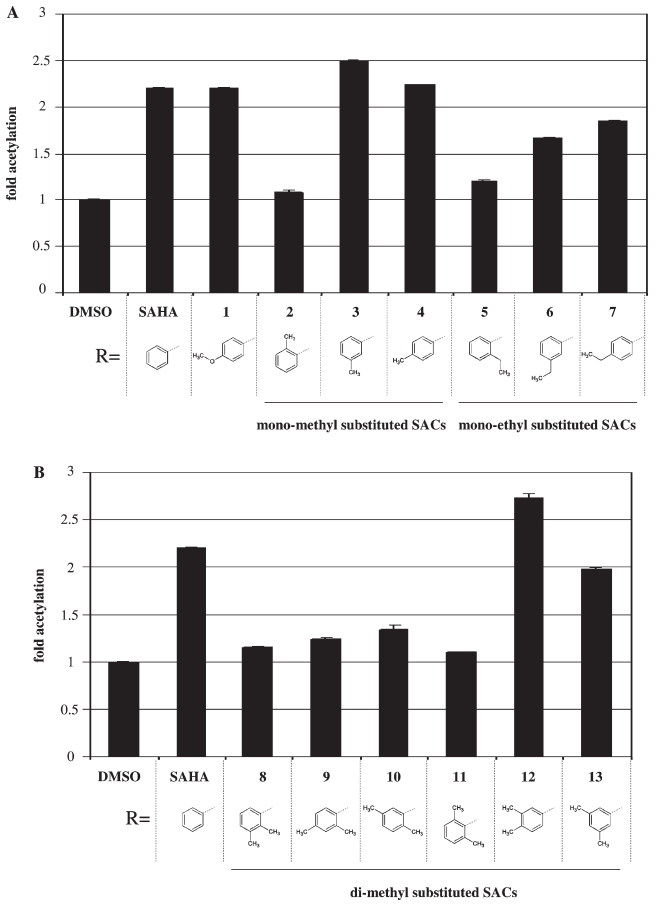

Figure 4. Quantitative analysis of protein acetylation levels in Caco-2 cells in response (A) to monomethyl- and monoethyl-substituted SACs treatments and (B) to dimethyl-substituted SACs treatments. Caco-2 cells were treated with a 5 μM concentration of the indicated compounds during 6 h, and indirect ELISA was performed in triplicate using 1 μg of whole cell protein extracts and anti acetyl-lysine as the primary antibody. Results are expressed as fold acetylation corresponding to protein acetylation level measured in response to indicated compounds as compared to the protein acetylation level measured using vehicle (DMSO). Error bars are standard deviations (SDs).

selectivity or specificity of SACs toward individual HDACs, we performed in vitro experiments with various recombinant HDACs. Two class 1 (HDAC1 and -3), two class 2a (HDAC5 and -7), and one class 2b (HDAC6) HDACs were used for these assays (dose−response curves are detailed in the Supporting Information, S4−S6). As shown in Table 2, all *o*-substituted compounds were less effective than SAHA at inhibiting class 1, 2a, and 2b HDACs. These data indicate that a single *o*-substitution is necessary and sufficient to dramatically reduce SAHA efficiency toward class 1 and class 2 HDACs. Conversely, methyl *m*- and *p*-substituted compounds (**3** and **4**) and ethyl *m*-substituted compound (**6**) were 1.3−3-fold more potent than SAHA (Table 2). Ethyl *p*-substituted compound (**7**) was as active as SAHA on all HDACs, except on HDAC7 (four times more efficient), suggesting some selectivity of this compound. Taken together, these data indicate that short alkyl chains, *m*- or *p*-substituted, may selectively potentiate SAHA-mediated inhibition of HDAC activity in vitro. Interestingly, crystallographic structures have revealed that the HDAC active site is surrounded by hydrophobic residues, which could provide targets for hydrophobic interactions involving alkyl chains substituted on the SAHA phenyl ring.[10,19−21] Remarkably, the dimethyl *m*- and *p*-substituted compound (**12**) and particulary the dimethyl *m*-substituted compound (**13**) were more potent on class 1 HDACs and on HDAC7, whereas their *o*-dimethyl counterpart (**11**) was the least active compound of the series on all tested HDACs. Because of the very high differential activity between **11** and **13**, we decided to explore further these compounds in structure−activity relationship (SAR) studies.

Molecular Modeling Reveals Proline 809 as a Potential Pharmacophore for the Design of Class 2 HDAC Selective Inhibitors. From the series of recombinant HDACs that we used for in vitro assay of SACs activity, HDAC7 is the only enzyme for which crystallographic data are available. Hence, to address structural features related to the contrasting biological efficiency of *o*- and *m*-dimethyl-substituted compounds (**11** and **13**, respectively), molecular modeling analyses were performed using SAHA, **11**, and **13** with HDAC7 (PDB ID: 3C0Z) as a template. As depicted in Figure 6A, SAHA was efficiently docked in the HDAC7 active site in a position allowing both interaction of the hydroxamic acid group with a Zn^{2+} atom and engagement of the NH from the amide group in a hydrogen bond with the carbonyl group of P809. Such a positioning of the HDACi is likely to be favored by interaction of the phenyl ring with F737. Interestingly, **13** was predicted to establish a similar hydrogen bond with P809, whereas **11**, most likely due to conformational constraints, had its NH group tilted away from P809 (Figure 6A). Through the analysis of the molecular dynamics runs of the three complexes, it appears that the lack of interaction between the NH group of **11** and the carbonyl group of the P809 may affect the interactions of the entire molecule with the protein active site. In particular, the hydroxamic moiety of **11** was predicted to adopt a different conformation in the zinc-binding pocket as compared to that of SAHA and **13** (Figure 6B). The root mean squared deviation (rmsd) of all three compounds calculated on the heavy atoms of truncated SAHA suggests that the binding of **11** is less stable than the other two ligands (Figure 6A). SAHA and **13** have a lower rmsd (calculated on the common structure atoms) than **11** and place their hydroxamic acid moiety in a very similar way as compared with TSA (not shown).

Similarly, molecular modeling of SAHA, **11**, and **13** in the active site of the other class 2a enzyme HDAC4 (PDB ID: 2VQW) suggested hydrogen bonding between the amide NH of SAHA and **13** and the carbonyl group of P942 (Supporting Information, S7). Accordingly, P942 of HDAC4 as well as P809 of HDAC7 are likely to be strong determinants of ligand binding. Examination of the solved HDAC4 and HDAC7 crystal structures in complex with HDACi revealed that these proline residues are indeed involved in the binding of compounds, although through bridging water molecules (Supporting Information, S8). Interestingly, proline at this position is only present in class 2 HDACs and thus provides a possible class-specific pharmacophore for drug targeting.

Substitution in *m*-Position Increases Compound Affinity for Recombinant HDAC7. Activity assays on recombinant HDAC enzymes with SACs indicated that *o*-substituted compounds (e.g., **11**) were 5−100-fold less efficient than SAHA, whereas dimethyl *m*- and/or *p*-substituted compounds (e.g., **13**) harbor not only a higher efficiency when compared to SAHA but also a partial enzymatic selectivity.

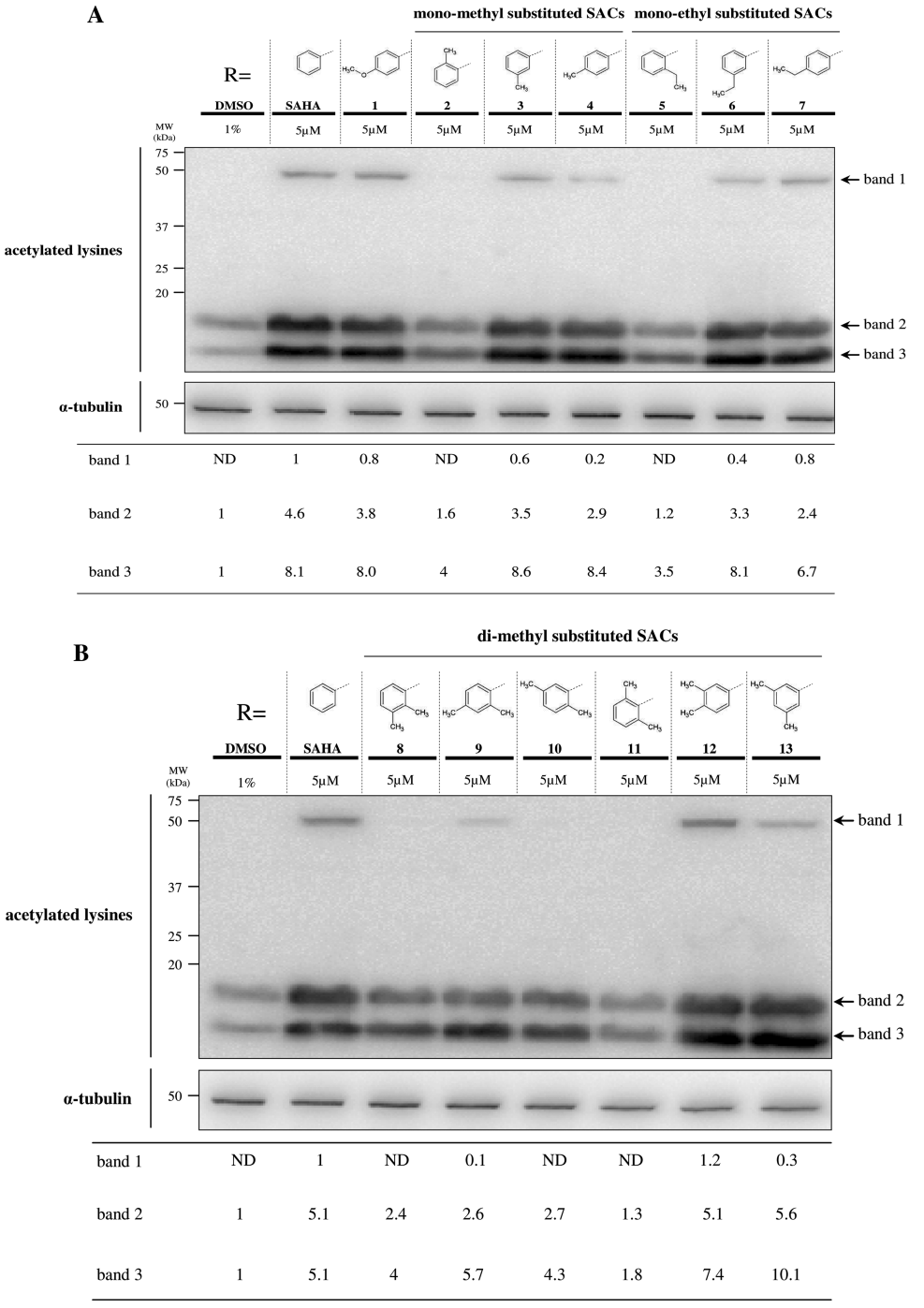

Figure 5. Protein acetylation profile in the soluble fraction of Caco-2 cells in response to (A) monomethyl- and monoethyl-substituted SACs treatments and (B) dimethyl-substituted SACs treatments. Caco-2 cells were treated with a 5 μM concentration of the indicated compounds during 6 h. α-Tubulin was used as a loading control. This result is representative of two independent experiments. When cells were treated with DMSO (1%) as a negative control, only two bands lower than 20 kDa were detectable (bands 2 and 3). The intensity of these bands was arbitrarily fixed to 1 to perform a densitometric analysis in comparison to SACs treatment. SAHA increased acetylation of at least one protein close to 50 kDa. As this signal was not detectable in the negative control, the intensity of this band was arbitrarily fixed to 1.

Although molecular modeling suggested structural clues for the explanation of the lack of activity of **11**, these analyses did not differentiate **13** from SAHA in terms of interaction. Thus, in an attempt to assess the SAR of compounds **11** and **13** in vitro, we performed saturation transfer difference (STD)[22] and water−ligand observation with gradient spectroscopy (WaterLOGSY)[23] NMR experiments using purified recombinant HDAC7 (aa 483−903). STD and WaterLOGSY sequences are known to be both particularly efficient for the screening of new molecules[24,25] and can be successfully applied to the analysis of mixtures of different ligands. Both methods rely on the existence of a strong negative nuclear Overhauser effect (NOE) associated with large molecules, in contrast with the weak positive NOE observed for free small molecules in solution. Hence, each ligand bound to a protein behaves as its large biomolecule partner and suffers long correlation time and negative NOE. STD corresponds to a direct transfer of magnetization

Table 2. SACs IC_{50} Values on Representative Class 1 (HDAC1 and HDAC3), Class 2a (HDAC5 and HDAC7), and Class 2b (HDAC6) HDACs[a]

	$IC_{50} \pm$ SEM (μM)				
	class 1		class 2a		class 2b
compounds	HDAC1	HDAC3	HDAC5	HDAC7	HDAC6
SAHA	0.119 ± 0.031	0.147 ± 0.053	12.60 ± 2.10	41.00 ± 10.20	0.037 ± 0.003
1	0.071 ± 0.011	0.137 ± 0.034	16.00 ± 3.30	21.60 ± 1.30	0.032 ± 0.002
2	0.576 ± 0.286	1.348 ± 0.002	42.70 ± 4.50	> 100	0.251 ± 0.069
3	0.057 ± 0.023	0.058 ± 0.032	11.30 ± 0.50	16.00 ± 1.80	0.030 ± 0.010
4	0.076 ± 0.026	0.114 ± 0.034	18.90 ± 2.70	19.00 ± 5.60	0.030 ± 0.001
5	1.101 ± 0.149	2.263 ± 0.427	> 100	> 100	0.215 ± 0.005
6	0.027 ± 0.002	0.035 ± 0.005	15.70 ± 4.10	16.10 ± 2.60	0.021 ± 0.001
7	0.149 ± 0.061	0.240 ± 0.070	9.60 ± 0.30	10.50 ± 1.60	0.026 ± 0.004
8	1.110 ± 0.240	1.750 ± 0.450	51.20 ± 12.20	> 100	0.206 ± 0.026
9	0.638 ± 0.013	1.100 ± 0.202	37.60 ± 6.10	45.40 ± 11.60	0.171 ± 0.002
10	1.142 ± 0.437	1.346 ± 0.164	54.30 ± 18.30	> 100	0.141 ± 0.041
11	11.614 ± 8.836	4.989 ± 1.051	> 100	> 100	0.615 ± 0.024
12	0.030 ± 0.010	0.056 ± 0.004	12.40 ± 0.50	15.90 ± 1.00	0.020 ± 0.001
13	0.017 ± 0.007	0.030 ± 0.001	14.30 ± 7.60	18.30 ± 7.30	0.035 ± 0.005

[a] IC_{50} values were determined from a minimum of two independent experiments. In each experiment, dose−response curves of compounds were tested in quadruplicate. The average IC_{50} values and the SEMs are reported in micromolar units.

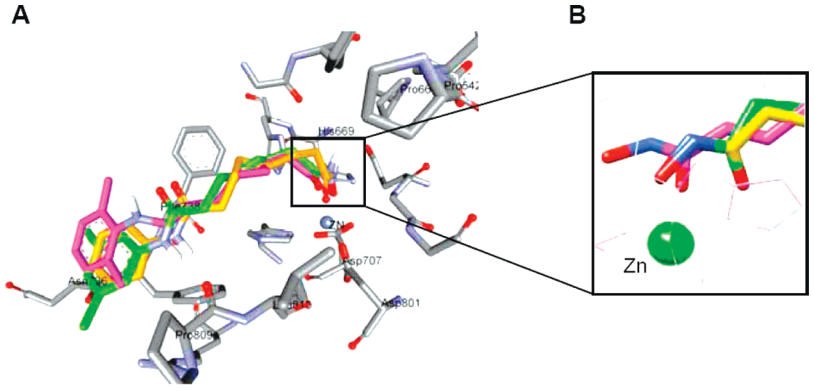

Ligand	RMSD (Å)	StdDev (Å)
SAHA	0.747	0.049
11	1.463	0.058
13	0.722	0.040

Figure 6. Molecular modeling of interaction between SAHA, compounds **11** and **13**, and the HDAC7 catalytic site. (A) SAHA (yellow) and compounds **11** (magenta) and **13** (green) are depicted in the HDAC7 active site (gray). Amino acids of the HDAC7 active site are indicated. The putative H-bond interaction between the proton of NH belonging to the amide function and the carbonyl group of proline 809 (P809) of HDAC7 is depicted as a green dotted line. (B) Close-up view of hydroxamic acid function. The table indicates the rmsd for each tested compound. The minimized average structure of SAHA (yellow) in complex with HDAC7 protein (gray) has been reported and is shown with the superimposition of **11** (magenta) and **13** (green) and belonging to the respective minimized average complex structures.

through the protein protons, whereas WaterLOGSY uses magnetization transfer through water molecules present at the protein−ligand interface. The results were visualized as a difference of spectra with and without magnetization transfer and are displayed in Figure 7 for SAHA, **11**, and **13**. Interestingly, the relative intensities of the aromatic resonances were no longer representative of an equimolar mixture in STD and WaterLOGSY assays (Figure 7A, e and f spectra, respectively). The signals corresponding to the *o*- (6.92 ppm) and *p*- (6.77 ppm) protons of **13** were stronger than the multiplet at 7.26 ppm related to the four *o*- and *m*-protons of SAHA. The multiplet centered at 7.03 ppm, which corresponds to three protons (*m*- and *p*-) of **11**, was only weakly detectable. Hence, these data indicate that the differential biological activities of **13**, SAHA, and **11** are likely related to their difference in binding to HDAC active sites. The weak affinity of **11** for HDAC7 catalytic domain when compared to **13** was confirmed through analysis of the methyl protons of both compounds (resonances at 2.13 and 2.01 ppm for **13** and **11**, respectively; Figure 7B). Again, despite being in equimolar concentration with **11** and SAHA, **13** generated the strongest signal. Hence, on the basis of all of the NMR data, we can rank affinity of these three ligands for HDAC7 in vitro as **13** > SAHA ≫ **11**.

These results indicate that a combination of two alkyl substituents in the *m*-position of the phenyl ring increases the potency of SAHA, likely through a stabilized interaction within the active site, and could lead to valuable new

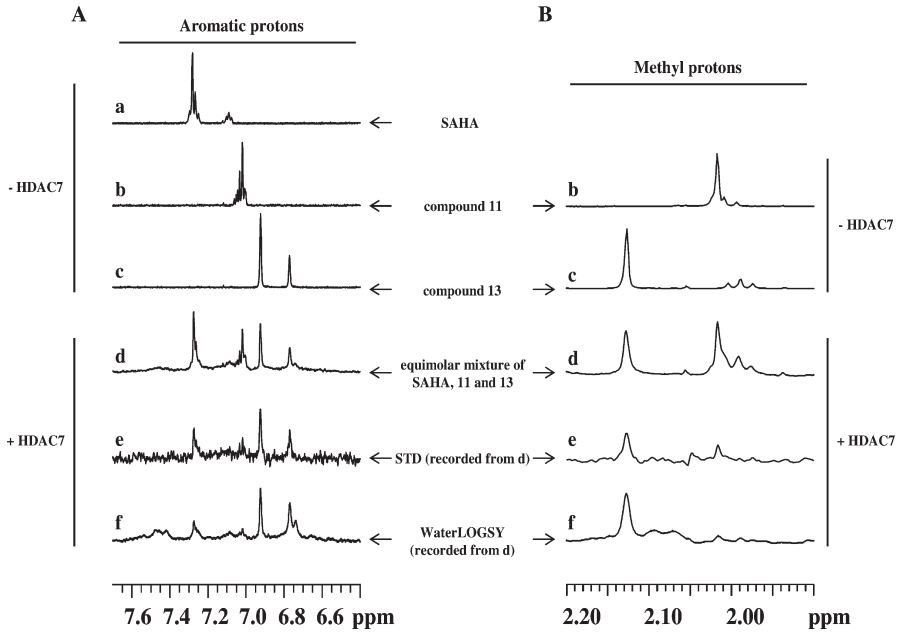

Figure 7. Expanded regions of one-dimensional spectra of (A) the aromatic protons of SAHA, compounds **11** and **13** (A), and the methyl protons (B). Experiments were performed in 20 mM phosphate buffer, pH 7.4, 100 mM NaCl, and 10% DMSO-d_6 and were recorded at 298 K. (a) SAHA, (b) compound **11**, (c) compound **13**, (d) equimolar mixture (60 μM) of the three ligands in the presence of 15 μM HDAC7, (e) STD spectrum recorded on sample d, and (f) WaterLOGSY spectrum recorded on sample d. All of the signals are presented arbitrary positive for convenience.

HDACi. In this context, the optimal combination and length of alkyl chains still remain to be determined. Accordingly, molecular modeling was performed using **13** docked in HDAC4 (PDB ID: 2VQW) as a reference and various compounds harboring from two to six carbon-length *m*-substituents (Supporting Information, S9). Results indicated that the number of different solutions increased with lengthening of the alkyl chain, revealing unconsistent positioning of the molecules within the active site. Consistent with the occurrence of variability in ligand position, the number of solutions relying on hydrogen bonding between the P942 and the amide NH decreased with chain length (Supporting Information, S9). A similar trend was observed when analyzing the position of the hydroxamic moiety of the compounds in proximity to the zinc ion (Supporting Information, S9). Hence, short chain derivatives are likely to group in the most active set of compounds.

Cell Growth Inhibitory Effects of SACs in Caco-2 Cancer Cells and in Nontumoral Cells. Because differential positioning of alkyl substituents on the SAHA phenyl ring differentially impacted HDACi effectiveness in vitro, we performed cell growth assays (3-[4,5-dimethylthiazol-2-yl]-2,5-diphenyltetrazolium bromide, MTT) to correlate these in vitro data to the growth inhibition profile of the various compounds in tumor cells. In parallel, we monitored $p21^{waf1/cip1}$ gene expression, a known SAHA-induced gene regulating cell cycle and apoptosis.[26] Caco-2 cells were treated during 48 h with increasing concentrations of SACs, SAHA, or vehicle only as a negative control. Mono *m*-substituted or *p*-substituted SACs (**3**, **4**, **6**, and **7**, respectively) showed IC_{50} values within the range of SAHA (Figure 8A). As monitored by Western blot, compounds **3**, **4**, **6**, and **7** also induced $p21^{waf1/cip1}$ expression in a dose-dependent manner similarly to SAHA (Figure 8A). Mono *o*-substituted SACs (**2** and **5**) were less efficient than SAHA with IC_{50} values approximately 5-fold higher than SAHA (78.5 and 40.5 μM, respectively). In agreement with these observations, $p21^{waf1/cip1}$ expression was barely induced by a 5 μM treatment with these compounds (Figure 8A). Nonetheless, at a concentration of 50 μM, *o*-substituted SACs **2**, **5**, **8**, and **11** were able to induce $p21^{waf1/cip1}$ expression (Supporting Information, S10). Taken together, these results suggest that mono *o*-substituted SACs are poor inhibitors of tumoral cell growth.

As shown in Figure 8A, dimethyl-substituted SACs harboring at least one *o*-substitution (**8**−**11**) exhibited higher IC_{50} values than SAHA in MTT assay. These high IC_{50} values were correlated to a lack of $p21^{waf/cip1}$ induction. Conversely, *m*-, *p*-dimethyl SACs (**12** and **13**) were as potent as SAHA in inhibiting cell growth and induced $p21^{waf1/cip1}$ to a similar extent (Figure 8A). Similar results were obtained with HepG2 cells (Supporting Information, S11), albeit **5** and **10** were more potent in inducing p21 expression in hepatoma cells than in Caco-2 cells. These observations indicate a strong correlation between the ability of these compounds to inhibit HDACs in vitro and in vivo and their ability to inhibit cell growth in cancer cells. Although IC_{50} values from **13** and SAHA were identical, dose−response curves were different and suggested that **13** is more potent than SAHA at concentrations ranging from 12.5 to 50 μM (Figure 8B). Indeed, Hill slopes were markedly different (−2.03 and −7.16 for SAHA and **13**, respectively), suggesting different modes of interaction with HDACs. The steepest slope observed with **13** could reflect a concentration-dependent stabilization of conformational transitions favoring binding of the inhibitor at high concentrations. Alternatively, binding of **13** to HDACs could induce phase transitions leading to enzyme aggregation, a phenomenon that could be interpreted as increased inhibition. However, slopes observed in in vitro inhibition assays with recombinant enzymes did not differ signicantly between SAHA and **13** (see the Supporting Information, S6), suggesting that the steepest slope observed in the presence of **13** in MTT assay might reflect cell-associated mechanisms.

A

Compound	R	Caco-2 cells: IC_{50} (μM)	Caco-2 cells: $p21^{waf1/cip1}$ induction (1 μM / 5 μM)
SAHA		8.1	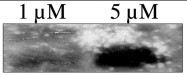
1	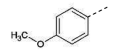	11.6	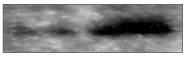
2		78.5	
3		10.7	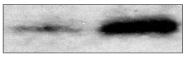
4	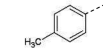	9.7	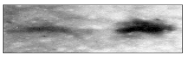
5		40.5	
6	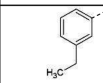	8.3	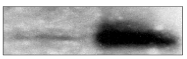
7	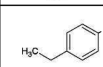	4.5	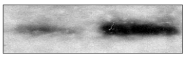
8	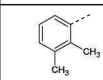	57.9	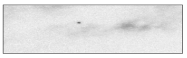
9	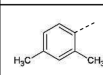	23.8	
10	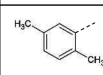	29.5	
11	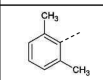	>100	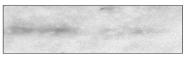
12	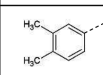	5.4	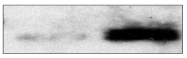
13	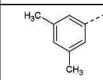	8	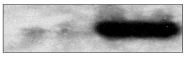

B

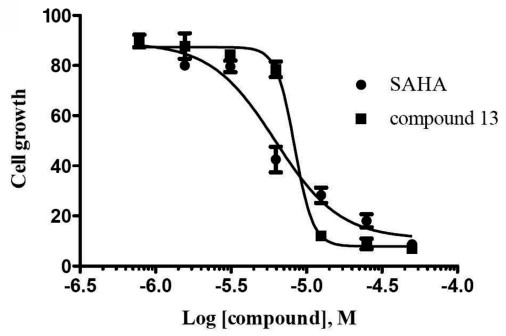

Figure 8. Growth inhibition assays (MTT) and $p21^{waf1/cip1}$ induction in response to SACs treatments in Caco-2 cells. (A) Cytotoxicity assays were performed using SACs concentrations ranging from 0.05 to 100 μM during 48 h of treatment. Results shown are representative of at least two independent experiments. $p21^{waf1/cip1}$ induction was analyzed after 1 or 5 μM SACs treatment during 24 h. IC_{50} = compound concentration leading to 50% of viable cells. $p21^{waf1/cip1}$ expression was monitored using Western blot after 24 h of treatment with 1 and 5 μM compounds. Equal loading between lanes was verified using antiactin antibodies (data not shown). (B) MTT dose−response curves for compound **13** and SAHA-treated Caco-2 cells.

Because **13** was more efficient than SAHA in several in vitro experiments and was partially more efficient in tumoral cell growth inhibition, we decided to compare **13** and SAHA activity toward growth of BJ and MUF nontumoral cells. Indeed, HDACi are known to be poor inducers of apoptosis in normal cells.[27] As expected, both HDACi had a moderate effect on nontumoral cell growth (Figure 9). Indeed, SAHA and **13** IC_{50} values could not be determined (> 100 μM). Cell growth was similarly affected by SAHA and **13** in BJ and MUF cells as judged from the almost superimposable dose−response curves (Figure 9). These data indicate that **13**, beside being more active than SAHA on several biological parameters, is not more detrimental than SAHA to normal cell growth, suggesting that **13** could be a potential candidate for further investigation.

Discussion

Distinguishing characteristics of HDACi include a metal binding moiety, a carbon linker, and a capping group. Considering SAHA, the molecule is characterized as having an anilide as a capping group, a $(CH_2)_6$ chain as a linker, and a hydroxamic group as a metal-chelating agent. On the basis of crystallographic analyses, the capping group is solvent-exposed and could potentially interact with amino acids near the entrance of the active site.[28] Most of the previous HDACi design have emphasized variations of the capping group of SAHA derivatives but with large modifications sampling the surface of the enzyme, such as changing the phenyl group to a benzyl group and adding functionalities in the α-position (α-aminosuberic acid).[29] In contrast, there is no systematic study involving discrete modifications of the phenyl ring while leaving the remainder of the molecule unchanged.

Our data demonstrate the importance of the position at which substituents are placed on the phenyl ring of SAHA. Indeed, *o*-substituted compounds were mostly inactive when compared to SAHA, whereas *m*- and *p*-substituted compounds were often more active than SAHA. The lack of potency of *o*-substituted compounds could be due to their low affinity for HDAC active sites. Indeed, although HDAC active sites might harbor a certain structural plasticity, as suggested by the recent resolution of HDAC4 crystallographic structure,[19] their surface might not be flexible enough to accommodate *o*-substitution of the SAHA phenyl ring.[10] Hence, the lack of potency of *o*-substituted compounds might not be due to steric constraints imposed by the protein moiety. Accordingly, molecular modeling did not reveal clashes between **11** and HDAC7 catalytic site. Interestingly, the collected data rather indicate that *o*-substitution might favor a particular compound conformation, altering both Zn^{2+} coordination and H-bond formation with the carbonyl group of P809. This amino acid, which is strictly conserved among class 2 HDACs only,[19] might be essential to stabilize the binding of HDACi, especially hydroxamic acids such as TSA and SAHA, in the active site of class 2 enzymes. Indeed, modeling data for SAHA and **13** indicate that Zn^{2+} is well-coordinated by the hydroxamic acid function and that the amide NH of SAHA and **13** could establish a H-bond with the carbonyl group of P809. Although molecular modeling allowed us to delineate structural features, which could explain the weak efficiency of *o*-substituted compounds, it did not explain the gain of potency of **13** on various biological parameters when compared to SAHA. However, STD and

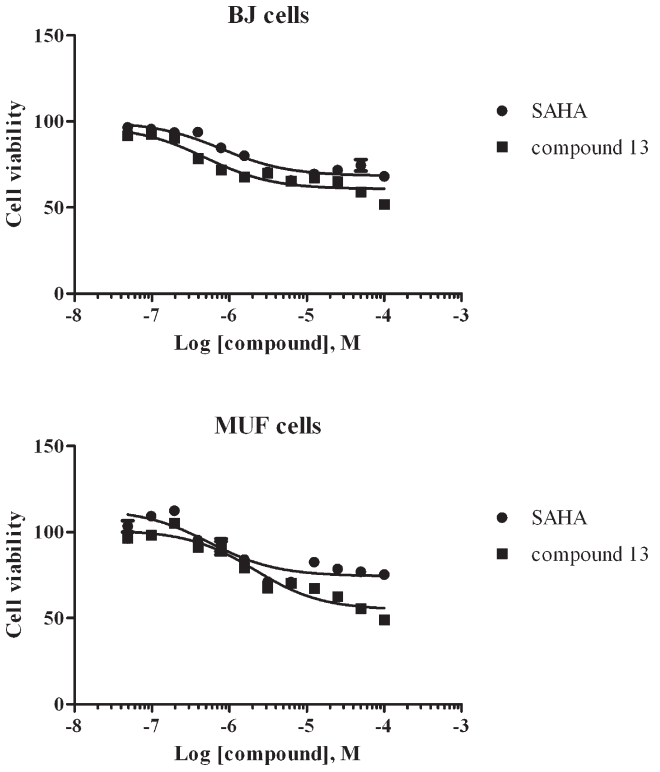

Figure 9. Growth of BJ and MUF nontumoral cells in the presence of SAHA and compound **13**. Cell growth assays were performed using SAHA and **13** concentrations ranging from 0.05 to 100 micromolar during 48 h of treatment.

WaterLOGSY NMR experiments indicated that **13** has a higher affinity for HDAC7 catalytic domain than SAHA. Indeed, analysis of NMR spectra suggested that the K_{off} (first-order dissociation rate constant) of **13** might be lower than the K_{off} of SAHA. Interestingly, although the cap group of SAHA is unresolved in the crystal structure of HDAC7, the protons do show interaction with the protein in STD experiments. This interaction seemed to be stronger when methyl groups were substituted in the *m*-position (**13**). The proximity of F737 to the phenyl ring of **13** could be involved in the strengthening of this interaction. Cocrystallization of HDAC7 with **13** would help to define the structural requirements for its binding to the catalytic site of the enzyme.

The key structural features of amides, especially short C−N bond lengths and hindered rotation about the C−N bond, have been extensively studied.[30] It is now well-established that the *E*/*Z* isomerism arises from delocalization of the lone pair of nitrogen into the π^* orbital of the carbonyl group with some double bond character and slow rotation. The barriers of rotation of amides have been studied mainly by nuclear magnetic resonance, but there are few studies of monosubstituted amides, due in part to the predominance of the *trans* form over the *cis* form.[31] In contrast, data for acetanilide derivatives are quite abundant, and the amount of *cis* isomer increases for acetanilides as the bulk of the *ortho*-substitution increases. For example, it has been reported that the *trans*/*cis* isomer ratio is >99 for acetanilide, 94/6 for 2-methylacetanilide, and 74/26 for 2,6-dimethylacetanilide. This increase in the *cis* isomer is paralleled by an increase in the barrier to rotation. Although a detailed explanation for the effects of varying the *o*-substituent is still missing, it was proposed that the *o*-substituted ring is out of the amide plane in the ground state and that this effect is amplified as the bulk of the *o*-substituent increases. In some cases, such as with 2,4,6-tri-*t*-butylacetanilide, a 55/45 (*trans*/*cis*) mixture of isomers is obtained, and the isomers can be separated. It is thus likely that *o*-substitution leads to SACs conformations that preclude a stable interaction with the enzymes and possibly to a decrease in the ability of the amide function to establish critical bonds within its immediate environment.

Conclusion

Our data provide clear evidence that minor modifications of the phenyl ring of SAHA can significantly change the properties of the inhibitor. Indeed, we report that the presence of alkyl groups in *o*-position (methyl or ethyl) decreases activity, whereas in *m*- and *p*-position, the presence of alkyl groups leads to a selective increase in activity, as revealed for **12** and **13**. In addition, we provide biophysical evidence that the increase in biological activity of **13** is correlated to an enhanced affinity of the compound toward the class 2 HDAC7 catalytic domain. Nevertheless, our understanding of the molecular mechanisms involved awaits structural information describing interaction between SACs and HDACs at the atomic level. Our data indicate that, when designing novel HDACi derived from SAHA, targeting the cap moiety may provide opportunities to develop more selective and/or more potent molecules, which could be used in physiopathological events such as hypercholesterolemia[32] or in various cancers.[33]

Experimental Section

Chemistry. All reactions were performed under argon. Solvents were distilled from the appropriate drying agent prior to use: tetrahydrofuran (THF) from sodium and benzophenone and MeOH from magnesium. Commercially available reagents were used without further purification unless otherwise stated. All reactions were monitored by TLC with Merck precoated aluminum foil sheets (Silica gel 60 with fluorescent indicator UV_{254}). Compounds were visualized with UV light at 254 and 365 nm. ^{1}H NMR and ^{13}C NMR were recorded using Bruker (Advance 300dpx and 200dpx) spectrometers at 300 (or 200 MHz) and 75 MHz (or 50 MHz), respectively. High-resolution mass spectra were recorded on a ZabSpec TOF Micromass spectrometer in ESI positive mode (compounds **1**−**13**), on a Varian MAT 311 Micromass spectrometer in EI mode (compounds **1a** and **3a**−**13a**) at the CRMPO (Centre Régional de Mesures Physiques de l'Ouest, University of Rennes), and on a Waters Q-TOF2 Micromass spectrometer in ESI positive mode (compound **2a**). Melting points were determined on a Kofler melting apparatus. All tested compounds are >95% pure by elemental analysis (Supporting Information, S12).

All of the syntheses of the SAHA derivatives were adapted from a method previously reported by Mai et al.[14] in three steps. The preparation of *N*-hydroxy-*N*′-(4-methylphenyl)octanediamide (AC22) (**4**) is described as a general example.

Suberic Anhydride (14). A solution of suberic acid (5.0 g, 28.7 mmol) in acetic anhydride (10 mL) was heated at reflux while it was stirred for 1 h. After it was cooled to room temperature, the solvent was evaporated under reduced pressure to give 4.40 g (98%) of a white solid (mp 52 °C). ^{1}H NMR (DMSO-d_6), white solid, mp 52 °C, δ (ppm): 1.34 (m, 4H, $H_{4,5}$), 1.62 (m, 4H, $H_{3,6}$), 2.41 (m, 4H, $H_{2,7}$).

8-[(4-Methylphenyl)amino]-8-oxooctanoic Acid (4a). 4-Methylaniline (343 mg, 3.21 mmol) was added to a stirred solution of suberic anhydride (500 mg, 3.21 mmol) in anhydrous THF. After it was stirred at room temperature for 30 min, the resulting mixture was filtered to give a solid as the bis-amide

(150 mg, 13%). The resulting filtrate was then diluted with water, yielding a white precipitate that was also filtered to give 370 mg (44%) of a white solid; mp 145 °C. ^{1}H NMR (DMSO-d_6) δ (ppm): 1.29 (m, 4H, $2H_4$, and $2H_5$), 1.53 (m, 4H, $2H_3$, and $2H_6$), 2.24 (m, 7H, CH_3−Ar, $2H_2$, and $2H_7$), 7.06 (d, 2H, 2H−Ar), 7.45 (d, 2H, 2H−Ar), 9.78 (s, 1H, NH). ^{13}C NMR (DMSO-d_6) δ (ppm): 21.3, 25.3, 25.9, 29.3, 34.5, 37.2, 39.1, 119.9, 129.9, 132.6, 137.7, 171.9, 175.4. MS: M^+ calcd for $C_{15}H_{21}NO_3$, 263.1521; found, 263.1510

***N*-Hydroxy-*N*′-(4-methylphenyl)octanediamide (4).** To a 0 °C cooled solution of 8-[(4-methylphenyl)amino]-8-oxooctanoic acid (**4a**) (370 mg, 1.41 mmol) in anhydrous THF, ethyl chloroformiate (213 mg, 1.97 mmol) and triethylamine (213 mg, 2.1 mmol) were added, and the mixture was stirred for 10 min. The solid was filtered off under argon, and the filtrate was added to freshly prepared solution of hydroxylamine in methanol. To prepare the hydroxylamine, a solution of hydroxylamine hydrochloride (293 mg, 4.22 mmol) in methanol (5 mL) was added to a stirred solution of potassium hydroxide (236 mg, 4.22 mmol) in methanol (5 mL) at 0 °C. After it was stirred for 15 min, the precipitate was removed, and the filtrate was used as such. The resulting mixture was stirred at room temperature for 15 min and then was evaporated. After the addition of 10 mL of acetonitrile to the residue, the solution was filtered to give a white solid of (**4**) (390 mg, 44%); mp 152 °C. ^{1}H NMR (DMSO-d_6) δ (ppm): 1.27 (m, 4H, $2H_4$, and $2H_5$), 1.52 (m, 4H, $2H_3$, and $2H_6$), 1.94 (m, 2H, $2H_7$), 2.27 (m, 5H, $2H_2$, and CH_3), 7.06 (d, 2H, 2Ar−H), 7.46 (d, 2H, 2Ar−H), 8.69 (s, 1H, OH), 9.80 (s, 1H, NH), 10.37 (s, 1H, NH). ^{13}C NMR (DMSO-d_6) δ (ppm): 21.3, 25.9, 29.3, 33.1, 37.2, 78.6, 119.9, 129.9, 132.6, 137.7, 169.9, 171.8. MS: $[M + Na]^+$ calcd for $C_{15}H_{22}N_2O_3Na$, 301.1528; found, 301.1526.

SAHA. White solid, mp 160 °C. ^{1}H NMR (DMSO-d_6) δ (ppm): 1.27 (m, 4H, $2H_4$, and $2H_5$), 1.52 (m, 4H, $2H_3$, and $2H_6$), 1.94 (m, 2H, $2H_7$), 2.29 (m, 2H, $2H_2$), 7.00 (m, 1H, Ar−H), 7.27 (m, 2H, 2Ar−H), 7.59 (d, 2H, 2Ar−H), 8.66 (s, 1H, OH), 9.92 (s, 1H, NH), 10.29 (s, 1H, NH).

***N*-Hydroxy-*N*′-(4-methoxyphenyl)octanediamide (1).** White solid (51%), mp 151 °C. ^{1}H NMR (DMSO-d_6) δ (ppm): 1.26 (m, 4H, $2H_4$, and $2H_5$), 1.50 (m, 4H, $2H_3$, and $2H_6$), 1.93 (m, 2H, $2H_7$), 2.25 (m, 2H, $2H_2$), 3.70 (m, 3H, OMe), 6.83 (d, 2H, 2Ar−H), 7.48 (d, 2H, 2Ar−H), 8.66 (s, 1H, OH), 9.78 (s, 1H, NH), 10.37 (s, 1H, NH). ^{13}C NMR (DMSO-d_6) δ (ppm): 25.9, 26.0, 29.3, 33.1, 37.1, 56.0, 114.6, 121.4, 133.5, 155.8, 170.0, 171.6. MS: $[M + Na]^+$ calcd for $C_{15}H_{22}N_2O_4Na$, 317.1477; found, 317.1477.

***N*-Hydroxy-*N*′-(2-methylphenyl)octanediamide (2).** White solid (38%), mp 135 °C. ^{1}H NMR (DMSO-d_6) δ (ppm): 1.31 (m, 4H, $2H_4$, and $2H_5$), 1.54 (m, 4H, $2H_3$, and $2H_6$), 1.95 (t, 2H, $2H_7$), 2.18 (s, 3H, CH_3), 2.32 (m, 5H, $2H_2$, and CH_3), 7.00−7.30 (m, 4H, 4Ar−H), 8.67 (s, 1H, OH), 9.23 (s, 1H, NH), 10.35 (s, 1H, NH). ^{13}C NMR (DMSO-d_6) δ (ppm): 18.7, 25.9, 26.1, 29.3, 33.1, 33.6, 36.6, 125.9, 126.1, 126.7, 131.1, 132.7, 137.3, 170.0, 172.0. MS: $[M + Na]^+$ calcd for $C_{15}H_{22}N_2O_3Na$, 301.1528; found, 301.1525.

***N*-Hydroxy-*N*′-(3-methylphenyl)octanediamide (3).** White solid (52%), mp 118 °C. ^{1}H NMR (DMSO-d_6) δ (ppm): 1.26 (m, 4H, $2H_4$, and $2H_5$), 1.48 (m, 2H, $2H_6$), 1.56 (m, 2H, $2H_3$), 1.93 (t, 2H, $2H_7$), 2.25 (m, 5H, $2H_2$, and CH_3), 6.83 (d, 1H, Ar−H), 7.14 (t, 1H, Ar−H), 7.36 (d, 1H, Ar−H), 7.43 (s, 1H, Ar−H), 8.66 (s, 1H, OH), 9.79 (s, 1H, NH), 10.33 (s, 1H, NH). ^{13}C NMR (DMSO-d_6) δ (ppm): 22.1, 25.9, 29.2, 33.1, 37.2, 117.1, 120.4, 124.5, 129.3, 138.6, 140.1, 169.9, 172.1. MS: $[M + Na]^+$ calcd for $C_{15}H_{22}N_2O_3Na$, 301.1528; found, 301.1523

***N*-(2-Ethylphenyl)-*N*′-hydroxyoctanediamide (5).** White solid (71%), mp 116 °C. ^{1}H NMR (DMSO-d_6) δ (ppm): 1.10 (t, 3H, $CH_2\mathbf{CH_3}$), 1.29 (m, 4H, $2H_4$, and $2H_5$), 1.53 (m, 4H, $2H_3$, and $2H_6$), 1.95 (t, 2H, $2H_7$), 2.31 (t, 2H, $2H_2$), 2.51 (q, 2H, $\mathbf{CH_2}CH_3$), 7.21 (m, 4H, 4Ar−H), 8.67 (s, 1H, OH), 9.30 (s, 1H, NH), 10.39 (s, 1H, NH). ^{13}C NMR (DMSO-d_6) δ (ppm): 15.2, 24.7, 25.9, 26.0, 26.2, 29.3, 33.2, 36.6, 122.5, 126.7, 127.2, 129.3, 136.7, 139.0, 170.0, 172.3. MS: $[M + Na]^+$ calcd for $C_{16}H_{24}N_2O_3Na$, 315.1685; found, 315.1680

Scheme 1. ^{1}H Atom-Labeling Used for SACs

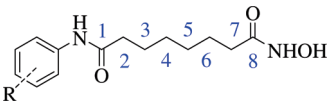

***N*-(3-Ethylphenyl)-*N*′-hydroxyoctanediamide (6).** White solid (62%), mp 120 °C. ^{1}H NMR (DMSO-d_6) δ (ppm): 1.15 (t, 3H, $CH_2\mathbf{CH_3}$), 1.26 (m, 4H, $2H_4$, and $2H_5$), 1.48 (m, 2H, $1H_3$, and $1H_6$), 1.55 (m, 2H, $1H_3$, and $1H_6$), 1.93 (m, 2H, $2H_7$), 2.27 (t, 2H, $2H_2$), 2.51 (q, 2H, $\mathbf{CH_2}CH_3$), 6.86 (d, 1H, Ar−H), 7.16 (t, 1H, Ar−H), 7.40 (d, 1H, Ar−H), 7.45 (s, 1H, Ar−H), 8.65 (s, 1H, OH), 9.86 (s, 1H, NH), 10.35 (s, 1H, NH). ^{13}C NMR (DMSO-d_6) δ (ppm): 16.5, 26.0, 29.2, 29.3, 33.1, 37.2, 117.4, 119.3, 123.3, 129.4, 140.3, 145.0, 170.0, 172.1. MS: $[M + Na]^+$ calcd for $C_{16}H_{24}N_2O_3Na$, 315.1685; found, 315.1673

***N*-(4-Ethylphenyl)-*N*′-hydroxyoctanediamide (7).** White solid (97%), mp 146 °C. ^{1}H NMR (DMSO-d_6) δ (ppm): 1.14 (t, 3H, $CH_2\mathbf{CH_3}$), 1.26 (m, 4H, $2H_4$, and $2H_5$), 1.49 (m, 4H, $2H_3$, and $2H_6$), 1.93 (m, 2H, $2H_7$), 2.27 (t, 2H, $2H_2$), 2,51 (q, 2H, $\mathbf{CH_2}CH_3$), 7.10 (d, 2H, 2Ar−H), 7.49 (d, 2H, 2Ar−H), 8.65 (s, 1H, OH), 9.84 (s, 1H, NH), 10.35 (s, 1H, NH). ^{13}C NMR (DMSO-d_6) δ (ppm): 21.3, 25.9, 29.3, 33.1, 37.2, 78.6, 119.9, 129.9, 132.6, 137.7, 169.9, 171.8. MS: $[M + Na]^+$ calcd for $C_{16}H_{24}N_2O_3Na$, 315.1685; found, 315.1692

***N*-(2,3-Dimethylphenyl)-*N*′-hydroxyoctanediamide (8).** White solid (50%), mp 129 °C. ^{1}H NMR (DMSO-d_6) δ (ppm): 1.30 (m, 4H, $2H_4$, and $2H_5$), 1.54 (m, 4H, $2H_3$, and $2H_6$), 1.95 (t, 2H, $2H_7$), 2.05 (s, 3H, CH_3), 2.24 (s, 3H, CH_3), 2.30 (t, 2H, $2H_2$), 7.03 (m, 3H, 3Ar−H), 8.68 (s, 1H, OH), 9.36 (s, 1H, NH), 10.40 (s, 1H, NH). ^{13}C NMR (DMSO-d_6) δ (ppm): 15.0, 21.1, 26.0, 26.2, 29.3, 33.2, 36.6, 124.6, 126.6, 127.6, 132.1, 137.1, 137.7, 170.2, 172.1. MS: $[M + Na]^+$ calcd for $C_{16}H_{24}N_2O_3Na$, 315.1685; found, 315.1685

***N*-(2,4-Dimethylphenyl)-*N*′-hydroxyoctanediamide (9).** White solid (57%), mp 117 °C. ^{1}H NMR (DMSO-d_6) δ (ppm): 1.30 (m, 4H, $2H_4$, and $2H_5$), 1.53 (m, 4H, $2H_3$, and $2H_6$), 1.95 (t, 2H, $2H_7$), 2.13 (s, 3H, CH_3), 2.24 (s, 3H, CH_3), 2.30 (t, 2H, $2H_2$), 6.94 (d, 1H, 1Ar−H), 6.99 (s, 1H, 1Ar−H), 7.19 (d, 1H, 1Ar−H), 8.67 (s, 1H, OH), 9.18 (s, 1H, NH), 10.37 (s, 1H, NH). ^{13}C NMR (DMSO-d_6) δ (ppm): 18.7, 21.6, 26.0, 26.2, 29.3, 33.1, 32.6, 39.1, 126.2, 127.2, 131.6, 132.7, 134.7, 134.9, 135.1, 170.0, 172.0. MS: $[M + Na]^+$ calcd for $C_{16}H_{24}N_2O_3Na$, 315.1685; found, 315.1688

***N*-(2,5-Dimethylphenyl)-*N*′-hydroxyoctanediamide (10).** White solid (52%), mp 134 °C. ^{1}H NMR (DMSO-d_6) δ (ppm): 1.30 (m, 4H, $2H_4$, and $2H_5$), 1.54 (m, 4H, $2H_3$, and $2H_6$), 1.95 (t, 2H, $2H_7$), 2.12 (s, 3H, CH_3), 2.24 (s, 3H, CH_3), 2.30 (t, 2H, $2H_2$), 6.87 (d, 1H, 1Ar−H), 7.05 (d, 1H, 1Ar−H), 7.17 (s, 1H, 1Ar−H), 8.67 (s, 1H, OH), 9.20 (s, 1H, NH), 10.37 (s, 1H, NH). ^{13}C NMR (DMSO-d_6) δ (ppm): 18.4, 21.5, 26.0, 26.2, 29.3, 33.1, 33.7, 122.5, 126.6, 129.5, 130.9, 135.7, 137.2, 170.0, 172.0. MS: $[M + Na]^+$ calcd for $C_{16}H_{24}N_2O_3Na$, 315.1685; found, 315.1678

***N*-(2,6-Dimethylphenyl)-*N*′-hydroxyoctanediamide (11).** White solid (95%), mp 133 °C. ^{1}H NMR (DMSO-d_6) δ (ppm): 1.31 (m, 4H, $2H_4$, and $2H_5$), 1.50 (m, 4H, $2H_3$, and $2H_6$), 1.95 (t, 2H, $2H_7$), 2.12 (s, 6H, CH_3), 2.30 (t, 2H, $2H_2$), 7.05 (s, 3H, 3Ar−H), 8.81 (s, 1H, OH), 9.23 (s, 1H, NH), 10.39 (s, 1H, NH). ^{13}C NMR (DMSO-d_6) δ (ppm): 19.0, 26.0, 26.3, 29.3, 29.4, 33.1, 36.2, 127.1, 128.5, 136.0, 136.3, 170.0, 171.7. MS: $[M + Na]^+$ calcd for $C_{16}H_{24}N_2O_3Na$, 315.1685; found, 315.1677

***N*-(3,4-Dimethylphenyl)-*N*′-hydroxyoctanediamide (12).** White solid (42%), mp 134 °C. ^{1}H NMR (DMSO-d_6) δ (ppm): 1.26 (m, 4H, $2H_4$, and t $2H_5$), 1.53 (m, 4H, $2H_3$, and $2H_6$), 2.16 (m, 10H, $2CH_3$, $2H_2$, and $2H_7$), 7.00 (d, 1H, Ar−H), 7.28 (d, 1H, Ar−H), 7.35(s, 1H, Ar−H), 8.66 (s, 1H, OH), 9.71 (s, 1H, NH), 10.35 (s, 1H, NH). ^{13}C NMR (DMSO-d_6) δ (ppm): 19.6, 20.5, 23.9, 26.0,

29.3, 33.1, 117.5, 121.2, 130.3, 131.4, 137.0, 138.0, 170.0, 171.9. MS: $[M + Na]^+$ calcd for $C_{16}H_{24}N_2O_3Na$, 315.1685; found, 315.1673

***N*-(3,5-Dimethylphenyl)-*N'*-hydroxyoctanediamide (13).** White solid (53%), mp 171 °C. ^{1}H NMR (DMSO-d_6) δ (ppm): 1.27 (m, 4H, $2H_4$, and $2H_5$), 1.51 (m, 4H, $2H_3$, and $2H_6$), 1.94 (t, 2H, $2H_7$), 2.21 (s, 6H, CH_3), 2.27 (t, 2H, $2H_2$), 6.65 (s, 1H, 1Ar−H), 7.22 (s, 2H, 2 Ar−H), 8.67 (s, 1H, OH), 9.76 (s, 1H, NH), 10.35 (s, 1H, NH). ^{13}C NMR (DMSO-d_6) δ (ppm): 22.0, 25.9, 26.0, 29.3, 33.1, 37.2, 117.7, 125.3, 138.4, 140.1, 170.0, 172.0. MS: $[M + Na]^+$ calcd for $C_{16}H_{24}N_2O_3Na$, 315.1685; found, 315.1677

8-[(4-Methoxyphenyl)amino]-8-oxooctanoic Acid (1a). White solid (21%), mp 144 °C. ^{1}H NMR (DMSO-d_6) δ (ppm): 1.29 (m, 4H, $2H_4$, and $2H_5$), 1.51 (m, 4H, $2H_3$, and $2H_6$), 2.22 (m, 4H, $2H_2$, and $2H_7$), 3.70 (s, 3H, OCH_3), 6.84 (m, 2H, 2Ar−H), 7.47 (m, 2H, 2Ar−H), 9.70 (s, 1H, NH). ^{13}C NMR (DMSO-d_6) δ (ppm): 25.3, 25.9, 29.2, 29.3, 34.5, 37.1, 56.0, 114.6, 121.4, 133.4, 155.8, 171.5, 175.4. MS: $[M + Na]^+$ calcd for $C_{15}H_{21}NO_4$, 279.1471; found, 279.1446

8-[(2-Methylphenyl)amino]-8-oxooctanoic Acid (2a). White solid (41%), mp 126 °C. ^{1}H NMR (DMSO-d_6) δ (ppm): 1.31 (m, 4H, $2H_4$, and $2H_5$), 1.53 (m, 4H, $2H_3$, and $2H_6$), 2.00−2.35 (m, 7H, $2H_2$, $2H_7$, and CH_3), 6.95−7.40 (m, 4H, 4Ar−H), 9.24 (s, 1H, NH). ^{13}C NMR (DMSO-d_6) δ (ppm): 18.7, 25.2, 26.1, 29.2, 34.5, 36.6, 126.0, 126.2, 126.7, 131.1, 132.7, 137.3, 172.1, 175.4. MS: M^+ calcd for $C_{15}H_{21}NO_3Na$, 286.1419; found, 286.1418

8-[(3-Methylphenyl)amino]-8-oxooctanoic Acid (3a). White solid (26%), mp 102 °C. ^{1}H NMR (DMSO-d_6) δ (ppm): 1.29 (m, 4H, $2H_4$, and $2H_5$), 1.53 (m, 4H, $2H_3$, and $2H_6$), 2.25 (m, 7H, $2H_2$, $2H_7$, and CH_3), 6.83 (d, 1H, Ar−H), 7.15 (t, 1H, Ar−H), 7.36 (d, 1H, Ar−H), 7.43 (s, 1H, Ar−H), 9.75 (s, 1H, NH). ^{13}C NMR (DMSO-d_6) δ (ppm): 22.1, 25.3, 25.9, 29.2, 29.3, 34.5, 37.2, 117.1, 120.4, 124.5, 129.3, 138.7, 140.1, 172.1, 175.4. MS: M^+ calcd for $C_{15}H_{21}NO_3$, 263.1521; found, 263.1510

8-[(2-Ethylphenyl)amino]-8-oxooctanoic Acid (5a). White solid (26%), mp 102 °C. ^{1}H NMR (DMSO-d_6) δ (ppm): 1.11 (t, 3H, $CH_2\mathbf{CH_3}$), 1.31 (m, 4H, $2H_4$, and $2H_5$), 1.55 (m, 4H, $2H_3$, and $2H_6$), 2.21 (t, 2H, $2H_7$), 2.31 (t, 2H, $2H_2$), 2.50 (q, 2H, $\mathbf{CH_2}CH_3$), 7.22 (m, 4H, 1Ar−H), 9.24 (s, 1H, NH). ^{13}C NMR (DMSO-d_6) δ (ppm): 16.5, 26.1, 26.7, 27.5, 30.6, 35.9, 37.9, 127.8, 128.1, 128.5, 130.7, 138.0, 140.3, 173.7, 176.8. MS: M^+ calcd for $C_{16}H_{23}NO_3$, 277.1678; found, 277.1686

8-[(3-Ethylphenyl)amino]-8-oxooctanoic Acid (6a). White solid (38%), mp 102 °C. ^{1}H NMR (DMSO-d_6) δ (ppm): 1.16 (t, 3H, $CH_2\mathbf{CH_3}$), 1.19 (m, 4H, $2H_4$, and $2H_5$), 1.54 (m, 4H, $2H_3$, and $2H_6$), 2.23 (m, 4H, $2H_2$, and $2H_7$), 2.54 (q, 2H, $\mathbf{CH_2}CH_3$), 6.86 (d, 1H, Ar−H), 7.18 (t, 1H, Ar−H), 7.41 (d, 1H, Ar−H), 7.44 (s, 1H, Ar−H), 9.79 (s, 1H, NH). ^{13}C NMR (DMSO-d_6) δ (ppm): 16.4, 25.3, 25.9, 29.2, 29.3, 34.5, 37.2, 117.3, 119.3, 123.3, 124.5, 129.4, 140.2, 145.0, 172.1, 175.4. MS: M^+ calcd for $C_{16}H_{23}NO_3$, 277.1678; found, 277.1686

8-[(4-Ethylphenyl)amino]-8-oxooctanoic Acid (7a). White solid (19%), mp 138 °C. ^{1}H NMR (DMSO-d_6) δ (ppm): 1.15 (t, 3H, $CH_2\mathbf{CH_3}$), 1.29 (m, 4H, $2H_4$, and $2H_5$), 1.53 (m, 4H, $2H_3$, and $2H_6$), 2.30 (m, 4H, $2H_2$, and $2H_7$), 2.53 (q, 2H, $\mathbf{CH_2}CH_3$), 7.11 (d, 2H, 2Ar−H), 7.48 (d, 2H, 2Ar−H), 9.77 (s, 1H, NH). ^{13}C NMR (DMSO-d_6) δ (ppm): 16.7, 25.3, 25.9, 29.2, 34.5, 37.2, 120.0, 128.7, 137.9, 139.1, 171.8, 175.4. MS: M^+ calcd for $C_{16}H_{23}NO_3$, 277.1678; found, 277.1686

8-[(2,3-Dimethylphenyl)amino]-8-oxooctanoic Acid (8a). White solid (42%), mp 142 °C. ^{1}H NMR (DMSO-d_6) δ (ppm): 1.32 (m, 4H, $2H_4$, and $2H_5$), 1.55 (m, 4H, $2H_3$, and $2H_6$), 2.05 (t, 3H, CH_3), 2.24 (m, 7H, $2H_2$, $2H_7$, and CH_3), 7.03 (m, 3H, 3Ar−H), 9.28 (s, 1H, NH). ^{13}C NMR (DMSO-d_6) δ (ppm): 14.9, 21.1, 25.3, 26.1, 29.2, 29.3, 34.6, 36.6, 124.6, 126.0, 127.7, 132.1, 137.1, 137.7, 172.0, 175.4. MS: M^+ calcd for $C_{16}H_{23}NO_3$, 277.1678; found, 277.1658

8-[(2,4-Dimethylphenyl)amino]-8-oxooctanoic Acid (9a). White solid (32%), mp 122 °C. ^{1}H NMR (DMSO-d_6) δ (ppm): 1.31 (m, 4H, $2H_4$, and $2H_5$), 1.51 (m, 4H, $2H_3$, and $2H_6$), 2.13 (s, 3H, CH_3), 2.17 (t, 2H, $2H_7$), 2.24 (s, 3H, CH_3), 2.28 (t, 2H, $2H_2$), 6.94 (d, 1H, 1Ar−H), 7.00 (s, 1H, 1Ar−H), 7.20 (d, 1H, Ar−H), 9.16 (s, 1H, NH). ^{13}C NMR (DMSO-d_6) δ (ppm): 18.7, 21.3, 25.3, 26.1, 26.2, 29.2, 29.3 29.4, 34.5, 36.5, 126.2, 127.2, 131.5, 132.6, 134.7, 135.0, 172.0, 175.4. MS: M^+ calcd for $C_{16}H_{23}NO_3$, 277.1678; found, 277.1686

8-[(2,5-Dimethylphenyl)amino]-8-oxooctanoic Acid (10a). White solid (48%), mp 128 °C. ^{1}H NMR (DMSO-d_6) δ (ppm): 1.31 (m, 4H, $2H_4$, and $2H_5$), 1.54 (m, 4H, $2H_3$, and $2H_6$), 2.13 (m, 5H, $2H_7$, and CH_3), 2.22 (m, 5H, $2H_2$, and CH_3), 6.88 (d, 1H, Ar−H), 7.06 (d, 1H, Ar−H), 7.17 (s, 1H, 1Ar−H), 9.17 (s, 1H, NH). ^{13}C NMR (DMSO-d_6) δ (ppm): 18.3, 21.5, 25.3, 26.1, 29.2, 29.3, 34.6, 36.6, 126.6, 129.5, 130.9, 135.7, 137.1, 172.0, 175.4. MS: M^+ calcd for $C_{16}H_{23}NO_3$, 277.1678; found, 277.1686

8-[(2,6-Dimethylphenyl)amino]-8-oxooctanoic Acid (11a). White solid (22%), mp 129 °C. ^{1}H NMR (DMSO-d_6) δ (ppm): 1.32 (m, 4H, $2H_4$, and $2H_5$), 1.55 (m, 4H, $2H_3$, and $2H_6$), 2.12 (s, 6H, CH_3), 2.21 (t, 2H, $2H_7$), 2.30 (t, 2H, $2H_2$), 7.05 (s, 3H, 3Ar−H), 9.18 (s, 1H, NH). ^{13}C NMR (DMSO-d_6) δ (ppm): 19.1, 25.3, 26.2, 29.2, 29.4, 34.5, 36.2, 127.1, 128.5, 136.0, 136.3, 171.6, 175.4. MS: M^+ calcd for $C_{16}H_{23}NO_3$, 277.1678; found, 277.1658

8-[(3,4-Dimethylphenyl)amino]-8-oxooctanoic Acid (12a). White solid (56%), mp 120 °C, ^{1}H NMR (DMSO-d_6) δ (ppm): 1.29 (m, 4H, $2H_4$, and $2H_5$), 1.53 (m, 4H, $2H_3$, and $2H_6$), 2.22 (m, 10H, 2 CH_3−Ar, $2H_2$, and $2H_7$), 7.00 (d, 1H, Ar−H), 7.32 (d, 1H, Ar−H), 7.36 (s, 2H, 2Ar−H), 9.69 (s, 1H, NH). ^{13}C NMR (DMSO-d_6) δ (ppm): 19.6, 20.5, 25.3, 25.9, 29.3, 34.5, 37.2, 117.5, 121.2, 130.3, 131.4, 137.0, 138.0, 171.8, 175.4. MS: M^+ calcd for $C_{16}H_{23}NO_3$, 277.1678; found, 277.1686

8-[(3,5-Dimethylphenyl)amino]-8-oxooctanoic Acid (13a). White solid (30%), mp 123 °C. ^{1}H NMR (DMSO-d_6) δ (ppm): 1.28 (m, 4H, $2H_4$, and $2H_5$), 1.53 (m, 4H, $2H_3$, and $2H_6$), 2.22 (m, 10H, $2H_2$, $2H_7$, and CH_3), 6.66 (s, 1H, 1Ar−H), 7.18 (s, 2H, 2Ar−H), 9.69 (s, 1H, NH). ^{13}C NMR (DMSO-d_6) δ (ppm): 22.0, 25.3, 26.0, 29.3, 34.5, 37.2, 117.7, 125.3, 138.4, 140.1, 172.0, 175.4. MS: M^+ calcd for $C_{16}H_{23}NO_3$, 277.1678; found, 277.1686

Cell Lines and Drug Treatment. All compounds (**1**−**13**, including SAHA) were dissolved in DMSO (dimethyl sulfoxide, Sigma) at 10 mM as a stock solution and stored at −20 °C. The Caco-2 cell line (ATCC number HTB-37), derived from a human colorectal adenocarcinoma, as well as HepG2 cell line (ATCC number HB-8065) were maintained under the conditions recommended by the suppliers at 37 °C and 5% CO_2. MUF is a primary cell line of human foreskin diploid fibroblasts created by Dr. Piršel (Cancer Research Institute, Slovak Academy of Sciences, Slovak Republic). Human fibroblasts BJ (ATCC number CRL-2522) were established from skin taken from normal foreskin. MUF and BJ cell lines were normal and nontransformed and, therefore, suitable as controls to tumor cell lines. MUF and BJ cell lines were cultured in DMEM supplemented with antibiotics and 10% fetal calf serum. For protein extract preparation and Western blotting analysis, cells were plated 1 day before drug treatment in six-well plates at a density of 3×10^5 cells per well. Cells were treated with desired compound at concentrations and times indicated in the figure captions.

Ex Vivo HDAC Activity. All compounds were evaluated for their ability to inhibit total HDAC activity ex vivo in Caco-2 cells using the HDAC Fluorimetric Cellular Activity Assay Kit (Biomol International) and employing TSA as a positive control. This assay is based on the use of Fluor de Lys fluorescent substrate, which is cell-permeable and a substrate for most class 1 and 2 HDACs. Caco-2 cells were seeded in triplicate in 96-well plates at a density of 3×10^4 cells per well and allowed to attach overnight (70% confluency). Media were replaced with 50 μL per well of media containing 200 μM Fluor de Lys substrate and 1 μM TSA as a positive control. Plates were incubated at 37 °C and 5% CO_2 for 4 h. To terminate HDAC activity and begin development of the fluorescence signal, 50 μL per well of the 1× Developer (Biomol International) diluted in cold lysis

buffer [50 mM Tris/HCl (pH 8.0), 137 mM NaCl, 2.7 mM KCl, 1 mM $MgCl_2$, and 1% NP-40] + 2 μM TSA was added and mixed by pipetting. After developer was added, plates were incubated for an additional 15 min at 37 °C, and the fluorescence was read (excitation 365 nm and emission 450 nm) in a microplate-reading fluorimeter (Fluorolite 1000, Dynatech Laboratories). Comparison of inhibited vs control relative fluorescence was employed to determine the percent HDAC activity remaining.

Indirect ELISA. Whole cell extracts were prepared using a Nuclear Extract Kit (Active Motif) according the manufacturer's instructions using TSA (1 μM) in each step to avoid protein deacetylation. Protein extracts (antigen) were diluted to a final concentration of 20 μg/mL in PBS, and wells of a PVC microtiter plate were coated with 1 μg of antigen. Plates were covered and incubated for 2 h at room temperature. Then, after the coating solution was removed, plates were washed three times by filling the wells with 200 μL of PBS. The solutions or washes were removed by flicking the plate over a sink. The remaining protein binding sites in the coated wells were blocked by adding 200 μL of blocking buffer [5% bovine serum albumin (BSA) in PBS] per well. Plates were covered and incubated for 2 h at room temperature. Plates were then washed twice with PBS, and 100 μL of antiacetyl lysines antibody (from rabbit, diluted 1/1000, Abcam) diluted in blocking buffer was added to each well. Plates were covered and incubated overnight at 4 °C. Subsequently, plates were washed four times with PBS, and 100 μL of conjugated secondary antibody (antirabbit, diluted 1/2500, Abcam) diluted in blocking buffer was added to each well. Then, plates were covered and incubated 2 h at room temperature. After four washes, the horseradish peroxidase (HRP) activity was measured using the colorimetric kit (Substrate Reagent Pack, R&D Systems) following the supplier's recommendations.

Western Blot Analysis. After the media were removed from six-well plates, cells were washed with PBS and harvested in 150 μL of PBS using a scraper. Protein concentrations were directly quantified in cell suspension using DC Protein Assay Kit (Biorad) according to the manufacturer's instructions. After centrifugation (5 min, 200*g*, 4 °C), cell pellets were resuspended in Laëmmli loading buffer to obtain the desired protein concentration. Then, samples were denatured by sonication (bioruptor, Diagenode, 7 min, 4 °C, max power) and boiling (10 min, 100 °C). In all Western blotting analyses, equal protein quantities were loaded on 12% SDS-PAGE, and electrophoresis separation was followed by proteins transfer on nitrocellulose membranes (Hybond-C Extra, Amersham Biosciences). The quality of protein transfer was systematically verified using red Ponceau staining (data not shown). Membranes were probed with appropriate primary antibodies in milk saturation buffer (PBS/0.1% Tween, 5% milk) for anti-$p21^{waf1/cip1}$ (from mouse, diluted 1/1000, Millipore), antiactin (from mouse, diluted 1/5000, Abcam), antiacetylated H3 (from rabbit, diluted 1/25000, Abcam), antihistone H3 (from rabbit, diluted 1/2000, Abcam), antiacetylated α-tubulin (from mouse, diluted 1/1000, Abcam), and anti-α-tubulin (from mouse, diluted 1/1000, Sigma) or in BSA saturation buffer (PBS/0.1% Tween, 5% BSA) for antiacetyl lysine (from rabbit, diluted 1/1000, Abcam). The secondary antibodies corresponding to antimouse (diluted 1/10000, Santa Cruz) or antirabbit (diluted 1/2500, Abcam) were coupled to HRP. The signal was enhanced by chemiluminescence using Immobilon (Millipore) as a substrate for HRP and detected on film (Biomax Film, Kodak) or camera (Biorad).

Compound Profiling on HDAC1, HDAC3, HDAC5, HDAC6, and HDAC7. HDAC1, HDAC3, and HDAC6 enzymes, HDAC substrates, HDAC buffer, and developer were from BPS Bioscience (San Diego, CA). Human HDAC5 and HDAC7 were recombinantly expressed in Sf9+ insect cells as chimeric fusions with N-terminal GST and C-terminal HIS tag and then purified by glutathione-sepharose and Ni-NTA Superflow chromatography. HDAC enzymes were diluted in HDAC buffer in the presence of 0.01% (w/v) BSA (Sigma) at the following working concentrations (1×): 75 nM HDAC1, 1 nM HDAC3, 1 nM HDAC5, 3 nM HDAC6, and 0.5 nM HDAC7. The respective enzyme concentrations were optimized to ensure the detection of the HDAC activities in the linear range of the reaction for at least 60 min, with a consumption of less than 10% of the initial substrate. Specific fluorogenic substrates were used at working concentrations equivalent to their respective $2 \times K_m$ values. In particular, the class 1 HDAC substrate (#50032) was used at 12 μM (HDAC1 and HDAC3), the class 2a HDAC substrate (#50040) was used at 4 μM (HDAC5 and HDAC7), while the specific HDAC6 substrate (#50037) was used at 30 μM. Compounds dissolved in DMSO were assayed in quadruplicate at 11 concentrations ranging from 0.316 nM to 31.6 μM for HDAC1, HDAC3, and HDAC6 and from 6.32 nM to 632 μM for HDAC5 and HDAC7. All of the dilution steps were robotically performed with a Matrix Control Mate (Thermo Scientific, Hudson, NH). The reaction was incubated for 45 min at 32 °C and stopped with developer 2× in the presence of 8 μM TSA (Sigma). Plates were further incubated at 32 °C for 30 min. The fluorescence intensity was detected with Safire2 (Tecan, Mannedorf, Switzerland) at gain 40 and with excitation−emission wavelengths of 353−450 nm, respectively. End point relative fluorescence units (RFU) data were transformed as a percentage of activity to compare the relative potency of the compounds on the different HDAC enzymes. Curve fitting was performed by GraphPad Prism 4.0, using a sigmoidal dose−response (variable slope) model. The average IC_{50} values were obtained as a minimum from two independent experiments (for details, see the Supporting Information, S4−S6).

Protein Expression and Purification of HDAC7. The catalytic domain of human HDAC7 (Uniprot: Q8WUI4; amino acids 483−903 with an expression-enhancing NASNNG C-terminal sequence) was expressed from a pET9-derived vector encoding an N-terminal TEV cleavable hexahistidine tag. *Escherichia coli* BL21 AI (Invitrogen) cotransformed with RIL plasmid (Stratagene) was used for protein expression. Protein was purified as described[19] with minor modifications (Supporting Information, S13).

Acquisition of NMR Spectra. All NMR spectra were recorded at 298 K with a spectral width of 14 ppm on Bruker Avance 500 MHz spectrometer, equipped with a 5 mm TXI inverse triple-resonance cryoprobe head. (PRISM platform, University of Rennes 1, France). Spectra processing was performed using TOPSPIN 1.3 software (Bruker). The in vitro experiments were performed as already described.[34]

STD Experiments. Selective saturation of the protein was achieved by a train of Gauss-shaped pulses of 50 ms length each, truncated at 1%, and separated by a 1 ms delay. Forty selective pulses were applied, leading to a total length of the saturation train of 2 s. The on-resonance irradiation of the protein was performed at a chemical shift of 1.3 ppm. Off-resonance irradiation was set at 40 ppm, where no protein signals were present. Unwanted magnetization water was suppressed using a WATERGATE 3-9-19 pulse sequence. A 30 ms spin lock pulse was applied to remove protein background signals. The total scan number in the STD experiments was 2000, acquired as 16 blocks of 128 scans each. The spectra on- and off-resonances were subtracted after multiplication by an exponential line-broadening function of 0.8 Hz prior to Fourier transformation.

WaterLOGSY Experiments. WaterLOGSY experiments were performed using a selective excitation with a 180° shaped pulse at H_2O position. The first water selective 180° pulse was applied during 5 ms. The first two pulsed field gradients (PFGs) had a typical duration of 2 ms. A weak rectangular PFG is applied during the entire length of the mixing time (1 s). A short gradient recovery time of 1 ms is applied at the end of the mixing time before the detection pulse. The water suppression in

both experiments was achieved with the excitation sculpting sequence. The data were collected with a sweep width of 14 ppm, an acquisition time of 0.585 s, and a relaxation delay of 2 s. Prior to Fourier transformation, the data were multiplied with an exponential function with a line-broadening of 0.8 Hz.

Molecular Modeling. Molecular modeling studies were performed with Macromodel 8[35] on a Intel Xeon dual core with Fedora Core 7 as the operating system. The OPLSAA-2001 force field[35,36] was applied for energy minimization and molecular dynamics simulation. Energy minimization protein−ligand complexes were performed with the conjugate gradient method[37] to an energy gradient of 0.001 kJ/(mol Å) with distant-dependent electrostatic treatment. The three ligands SAHA, **11**, and **13** were built by the Build tool and energy minimized with previous force field and parameters.

Protein−Ligand Complex Simulations. The crystals complexes HDAC7−SAHA (PDB ID: 3C0Z) and HDAC7−TSA (PDB ID: 3C10) have been downloaded from the public RCSB Protein Data Bank (www.rcdb.org).[38] The chains A of all complexes were used for all of the simulations. In all three complexes of HDAC7−SAHA, the ligands were not completely resolved, and particularly, the *N*-phenylacetamide was not present. This precludes evaluation of the interactions of the *N*-phenylacetamide moiety with the amino acids of the protein, and using the complex HDAC7−SAHA with a truncate ligand in the preliminary minimization phases could bring partial occlusion of the entrance of the cavity by the closest amino acids side chains. After these considerations from both crystal cells, the two A chains have been selected and superimposed (rmsd on the heavy atoms of the backbone was 0.134 Å) to evaluate the peculiar differences in the amino acid side chain orientations or in the tertiary structure near the binding cavity and in the receptor surface close to the entrance of the cavity. After this checking phase, where no important differences were found, the chain A of the complex HDAC7−TSA was selected for the successive simulations. All hydrogens were inserted into the structure of chain A of 3C10 complex, all water molecules were removed, the $N^{\delta}H$ tautomer of the H709 was chosen, and a partial charge of +2 was assigned to the zinc ions. The chain A, with TSA, was energetically minimized with OPLSAA-2001 force field keeping the entire backbone fixed. The TSA ligand was removed from the minimized complex, and the truncated SAHA has been introduced as a guideline for the successive insertion of the complete SAHA, **11**, and **13**. The three complexes HDAC7−SAHA, HDAC7−**11**, and HDAC7−**13** were generated, and their energies were minimized. All of the minimum energy conformations of the complexes were submitted to dynamic simulations with the OPLSAA-2001 force field at 300 K, with an 10 ps of equilibration, and 100 ps of production time with a time step of 1 fs collecting 100 snapshots every 1 ps. Only the amino acid side chains inside a sphere of 5 Å from the ligand were free to move, while the rest of the amino acid side chains and the entire backbone were kept fixed. The average structures obtained from 10 representative snapshots of MD trajectory were energy minimized with the OPLSAA-2001 force field to a gradient of 0.001 kJ/(mol Å), with a fixed protein backbone.

Growth Inhibition Assays. One day prior to treatment, Caco-2, HepG2, and normal human fibroblast cells (MUF and BJ cells) were plated on 96-well plates in appropriate media, at densities of 2.104 cells/well for Caco-2 and HepG2 cells and 4.103 cells/well for MUF and BJ cells. Cells were exposed to the tested compounds for 48 h at concentrations ranging from 100 to 0.05 μM with 2-fold dilutions. DMSO was used as a negative control with the same dilutions starting from 1%. After treatment for 48 h, 10 μL of MTT (thiazolyl blue, 5 mg/mL) was added to each well and cultured for 2 h. Then, after the media were removed, formazan crystals were dissolved in 100 μL of DMSO. The absorbance was measured at 570 nm, and the background was measured at 630 nm using a microplate reader (Power Wave X5; Biotek). Data were acquired using KC4 version 3.4 software (Biotek Instruments Inc.). Results (% of cell growth) were calculated as follows: $[(A_{570} - A_{630})_{compound}/(A_{570} - A_{630})_{DMSO}] \times 100$. Results were averaged from three independent experiments for Caco-2 cells and from at least six independent experiments for BJ and MUF cells. Curve fitting was performed by GraphPad Prism 4.0.

Acknowledgment. We thank Maud Bizot and Gaëlle Palierne for technical assistance. We thank Jean-François Geffroy, Anne-Sophie Julien, Alicia Cassant, and Elodie Guiheux for their technical support. We thank Dr. Jérome Eeckhoute for his precious help with the writing of the manuscript. MUF cells were kindly provided by Dr. Miroslav Piršel. This work was funded by the European Community (LSHM-CT-2006-037498), the Région Bretagne (SIE 211-B3-11), the Centre National pour la Recherche Scientifique, and the Ministère de l'Enseignement Supérieur et de la Recherche.

Supporting Information Available: Acetylation level of histones H3/H4 and α-tubulin in response to SACs treatment (S1), materials and methods for histone preparation (S2), Western blot analysis of protein acetylation in HepG2 cells treated with SACs (S3), compound handling and pipetting scheme for compound profiling (S4), Z' factor evaluation[39] (S5), dose−reponse curves on HDAC1, -3, -5, -6, and -7 using SACs compounds (S6), modeling experiments suggesting a conserved protein−ligand interaction mode between the cap domain of SAHA and class 2 HDACs, method for HDAC4−SACs complex modeling (S7), importance of HDAC7 proline 809 and HDAC4 proline 274 for ligand interaction (S8), lengthening of the carbon chain on the phenyl ring of SAHA leading to eratic docking (S9), $p21^{waf1/cip1}$ induction in response to increasing concentrations (5, 50, and 100 μM) of representative *o*-substituted SACs (S10), MTT assay and $p21^{waf1/cip1}$ induction in HepG2 cells treated with SACs (S11), table of RP-HPLC purity and microanalytical data (S12), and complete material and methods for recombinant HDAC7 preparation and purification (S13). This material is available free of charge via the Internet at http://pubs.acs.org.

References

(1) Yang, X. J.; Seto, E. The Rpd3/Hda1 family of lysine deacetylases: from bacteria and yeast to mice and men. *Nat. Rev. Mol. Cell Biol.* **2008**, *9*, 206–218.
(2) Michan, S.; Sinclair, D. Sirtuins in mammals: Insights into their biological function. *Biochem. J.* **2007**, *404*, 1–13.
(3) Lu, Q.; Qiu, X.; Hu, N.; Wen, H.; Su, Y.; Richardson, B. C. Epigenetics, disease, and therapeutic interventions. *Ageing Res. Rev.* **2006**, *5*, 449–467.
(4) Paris, M.; Porcelloni, M.; Binaschi, M.; Fattori, D. Histone deacetylase inhibitors: from bench to clinic. *J. Med. Chem.* **2008**, *51*, 1505–1529.
(5) Bolden, J. E.; Peart, M. J.; Johnstone, R. W. Anticancer activities of histone deacetylase inhibitors. *Nat. Rev. Drug. Discovery* **2006**, *5*, 769–784.
(6) Mai, A.; Massa, S.; Lavu, S.; Pezzi, R.; Simeoni, S.; Ragno, R.; Mariotti, F. R.; Chiani, F.; Camilloni, G.; Sinclair, D. A. Design, Synthesis, And Biological Evaluation of Sirtinol Analogues as Class III Histone/Protein Deacetylase (Sirtuin) Inhibitors. *J. Med. Chem.* **2005**, *48*, 7789–7895.
(7) Marks, P. A.; Breslow, R. Dimethyl sulfoxide to vorinostat: Development of this histone deacetylase inhibitor as an anticancer drug. *Nat. Biotechnol.* **2007**, *25*, 84–90.
(8) Miller, T. A.; Witter, D. J.; Belvedere, S. Histone Deacetylase Inhibitors. *J. Med. Chem.* **2003**, *46*, 5097–5116.
(9) Finnin, M. S.; Donigian, J. R.; Cohen, A.; Richon, V. M.; Rifkind, R. A.; Marks, P. A.; Breslow, R.; Pavletich, N. P. Structures of a histone deacetylase homologue bound to the TSA and SAHA inhibitors. *Nature* **1999**, *401*, 188–193.
(10) Vannini, A.; Volpari, C.; Filocamo, G.; Casavola, E. C.; Brunetti, M.; Renzoni, D.; Chakravarty, P.; Paolini, C.; De Francesco, R.;

Gallinari, P.; Steinkuhler, C.; Di Marco, S. Crystal structure of a eukaryotic zinc-dependent histone deacetylase, human HDAC8, complexed with a hydroxamic acid inhibitor. *Proc. Natl. Acad. Sci. U.S.A.* **2004**, *101*, 15064–15069.
(11) Monneret, C. Histone deacetylase inhibitors. *Eur. J. Med. Chem.* **2005**, *40*, 1–13.
(12) Andrianov, V.; Gailite, V.; Lola, D.; Loza, E.; Semenikhina, V.; Kalvinsh, I.; Finn, P.; Petersen, K. D.; Ritchie, J. W.; Khan, N.; Tumber, A.; Collins, L. S.; Vadlamudi, S. M.; Bjorkling, F.; Sehested, M. Novel amide derivatives as inhibitors of histone deacetylase: design, synthesis and SAR. *Eur. J. Med. Chem.* **2009**, *44*, 1067–1085.
(13) Estiu, G.; Greenberg, E.; Harrison, C. B.; Kwiatkowski, N. P.; Mazitschek, R.; Bradner, J. E.; Wiest, O. Structural Origin of Selectivity in Class II-Selective Histone Deacetylase Inhibitors. *J. Med. Chem.* **2008**, *51*, 2898–2906.
(14) Mai, A.; Esposito, M.; Sbardella, G.; Massa, S. A new facile and expeditious synthesis of N-hydroxy-N′-phenyloctanediamide, a potent inducer of terminal cytodifferentiation. *OPPI Briefs* **2001**, *33*, 391–394.
(15) Codd, R. Coordination chemistry of hydroxamic acid. *Coord. Chem. Rev.* **2008**, *252*, 1387–1408.
(16) Lea, M. A.; Ibeh, C.; Shah, N.; Moyer, M. P. Induction of differentiation of colon cancer cells by combined inhibition of kinases and histone deacetylase. *Anticancer Res.* **2007**, *27*, 741–748.
(17) Mariadason, J. M. HDACs and HDAC inhibitors in colon cancer. *Epigenetics* **2008**, *3*, 28–37.
(18) Khan, N.; Jeffers, M.; Kumar, S.; Hackett, C.; Boldog, F.; Khramtsov, N.; Qian, X.; Mills, E.; Berghs, S. C.; Carey, N.; Finn, P. W.; Collins, L. S.; Tumber, A.; Ritchie, J. W.; Jensen, P. B.; Lichenstein, H. S.; Sehested, M. Determination of the class and isoform selectivity of small-molecule histone deacetylase inhibitors. *Biochem. J.* **2008**, *409*, 581–589.
(19) Bottomley, M. J.; Lo Surdo, P.; Di Giovine, P.; Cirillo, A.; Scarpelli, R.; Ferrigno, F.; Jones, P.; Neddermann, P.; De Francesco, R.; Steinkuhler, C.; Gallinari, P.; Carfi, A. Structural and functional analysis of the human HDAC4 catalytic domain reveals a regulatory structural zinc-binding domain. *J. Biol. Chem.* **2008**, *283*, 26694–26704.
(20) Schuetz, A.; Min, J.; Allali-Hassani, A.; Schapira, M.; Shuen, M.; Loppnau, P.; Mazitschek, R.; Kwiatkowski, N. P.; Lewis, T. A.; Maglathin, R. L.; McLean, T. H.; Bochkarev, A.; Plotnikov, A. N.; Vedadi, M.; Arrowsmith, C. H. Human HDAC7 harbors a class IIa histone deacetylase-specific zinc binding motif and cryptic deacetylase activity. *J. Biol. Chem.* **2008**, *283*, 11355–11363.
(21) Somoza, J. R.; Skene, R. J.; Katz, B. A.; Mol, C.; Ho, J. D.; Jennings, A. J.; Luong, C.; Arvai, A.; Buggy, J. J.; Chi, E.; Tang, J.; Sang, B. C.; Verner, E.; Wynands, R.; Leahy, E. M.; Dougan, D. R.; Snell, G.; Navre, M.; Knuth, M. W.; Swanson, R. V.; McRee, D. E.; Tari, L. W. Structural snapshots of human HDAC8 provide insights into the class I histone deacetylases. *Structure* **2004**, *12*, 1325–1334.
(22) Meyer, B.; Peters, T. NMR spectroscopy techniques for screening and identifying ligand binding to protein receptors. *Angew. Chem., Int. Ed. Engl.* **2003**, *42*, 864–890.
(23) Dalvit, C.; Pevarello, P.; Tato, M.; Veronesi, M.; Vulpetti, A.; Sundstrom, M. Identification of compounds with binding affinity to proteins via magnetization transfer from bulk water. *J. Biomol. NMR* **2000**, *18*, 65–68.
(24) Fielding, L. NMR methods for the determination of protein-ligand dissociation constants. *Prog. Nucl. Magn. Reson. Spectrosc.* **2007**, *51*, 219–242.
(25) Pellecchia, M.; Bertini, I.; Cowburn, D.; Dalvit, C.; Giralt, E.; Jahnke, W.; James, T. L.; Homans, S. W.; Kessler, H.; Luchinat, C.; Meyer, B.; Oschkinat, H.; Peng, J.; Schwalbe, H.; Siegal, G. Perspectives on NMR in drug discovery: A technique comes of age. *Nat. Rev. Drug Discovery* **2008**, *7*, 738–745.
(26) Ocker, M.; Schneider-Stock, R. Histone deacetylase inhibitors: signalling towards p21cip1/waf1. *Int. J. Biochem. Cell Biol.* **2007**, *39*, 1367–1374.
(27) Kelly, W. K.; Marks, P. A. Drug insight: Histone deacetylase inhibitors-development of the new targeted anticancer agent suberoylanilide hydroxamic acid. *Nat. Clin. Pract. Oncol.* **2005**, *2*, 150–157.
(28) Dowling, D. P.; Gantt, S. L.; Gattis, S. G.; Fierke, C. A.; Christianson, D. W. Structural Studies of Human Histone Deacetylase 8 and Its Site-Specific Variants Complexed with Substrate and Inhibitors. *Biochemistry* **2008**, *47*, 13554–13563.
(29) Kahnberg, P.; Lucke, A. J.; Glenn, M. P.; Boyle, G. M.; Tyndall, J. D. A.; Parsons, P. G.; Fairlie, D. P. SAHA from α-Aminosuberic Acid. *J. Med. Chem.* **2006**, *49*, 7611–7622.
(30) Avalos, M.; Babiano, R.; Barneto, J. L.; Bravo, J. L.; Cintas, P.; Jimenez, J. L.; Palacios, J. C. Can We Predict the Conformational Preference of Amides. *J. Org. Chem.* **2001**, *66*, 7275–7282.
(31) Stewart, W. E.; Siddall, T. H., III. Nuclear Magnetic Resonance Studies of Amides. *Chem. Rev.* **1970**, *70*, 517–551.
(32) Mitro, N.; Godio, C.; De Fabiani, E.; Scotti, E.; Galmozzi, A.; Gilardi, F.; Caruso, D.; Vigil Chacon, A. B.; Crestani, M. Insights in the regulation of cholesterol 7alpha-hydroxylase gene reveal a target for modulating bile acid synthesis. *Hepatology* **2007**, *46*, 885–897.
(33) Witt, O.; Deubzer, H. E.; Milde, T.; Oehme, I. HDAC family: What are the cancer relevant targets? *Cancer Lett.* **2009**, *277*, 8–21.
(34) Le Guevel, R.; Oger, F.; Lecorgne, A.; Dudasova, Z.; Chevance, S.; Bondon, A.; Barath, P.; Simonneaux, G.; Salbert, G. Identification of small molecule regulators of the nuclear receptor HNF4alpha based on naphthofuran scaffolds. *Bioorg. Med. Chem.* **2009**, *17*, 7021–7030.
(35) Mohamadi, F.; Richards, N. G. J.; Guida, W. C.; Liskamp, R.; Lipton, M.; Caufield, C.; Chang, G.; Hendrickson, T.; Still, W. C. An integrated software for modeling organic and bioorganic molecules using molecular mechanics. *J. Comput. Chem.* **1990**, *11*, 440–467.
(36) Jorgensen, W. L.; Maxwell, D. S.; Tirado-Rives, J. Development and Testing of the OPLS All-Atom Force Field on Conformational Energetics and Properties of Organic Liquids. *J. Am. Chem. Soc.* **1996**, *118*, 11225–11236.
(37) Polak, E.; Ribière, G. Note sur la convergence de directions conjuguées. *Rev. Fr. Informat. Rech. Operationelle* **1969**, *16*, 35–43.
(38) Berman, H. M.; Westbrook, J.; Feng, Z.; Gilliland, G.; Bhat, T. N.; Weissig, H.; Shindyalov, I. N.; Bourne, P. E. The Protein Data Bank. *Nucleic Acids Res.* **2000**, *28*, 235–42.
(39) Zhang, J. H.; Chung, T. D.; Oldenburg, K. R. A Simple Statistical Parameter for Use in Evaluation and Validation of High Throughput Screening Assays. *J. Biomol. Screening* **1999**, *4*, 67–73.